REPORT DOCUMENTATION PAGE

Form Approved
OMB No. 0704-0188

1. AGENCY USE ONLY (Leave blank)	2. REPORT DATE	3. REPORT TYPE AND DATES COVERED
	16 January 1997	Final 1 January 1994 - 31 March 1996

4. TITLE AND SUBTITLE

Fine-Scale Record of Faulting in ONR Natural Laboratories

5. FUNDING NUMBERS

G N00014-94-1-0466

6. AUTHOR(S)

Brian E. Tucholke, Gary E. Jaroslow, W. Kenneth Stewart and Martin C. Kleinrock

7. PERFORMING ORGANIZATION NAME(S) AND ADDRESS(ES)

Woods Hole Oceanographic Institution
Woods Hole, MA 02543

8. PERFORMING ORGANIZATION REPORT NUMBER

130466SP

9. SPONSORING / MONITORING AGENCY NAME(S) AND ADDRESS(ES)

Office of Naval Research
800 North Quincy Street
Arlington, VA 22217

10. SPONSORING / MONITORING AGENCY REPORT NUMBER

11. SUPPLEMENTARY NOTES

12a. DISTRIBUTION / AVAILABILITY STATEMENT

Approved for public release; distribution is unlimited.

12b. DISTRIBUTION CODE

13. ABSTRACT *(Maximum 200 words)*

We analyzed fault patterns in ocean crust on the west flank of the Mid-Atlantic Ridge at 25°25' - 27°10'N, 45°00' - 49°00'W, using HMR1 long-range sidescan-sonar data and multibeam bathymetry. Our studies show that brittle strain on normal faults varies with respect to intrasegment tectonic setting and with respect to variation in magma input at the rift axis. Our analyses clearly document that patterns of inward- and outward-facing normal faults account for the shape of the rift valley in slow-spreading crust, and they show that these faults control typical abyssal-hill morphology. We also analyzed near-bottom, fine-scale survey data and demonstrated for the first time that fault scarps in igneous ocean crust experience extensive, long-term denudation (10-20 m.y. off axis). We developed analytical techniques that will be widely applicable to analysis of sonar data from all ocean environments. The insights into basement roughness and backscatter patterns from ocean crust gained from this study also directly benefitted efforts to understand acoustic reverberation from the ocean bottom and subbottom within ONR's Acoustic Reverberation Special Research Program.

14. SUBJECT TERMS	15. NUMBER OF PAGES
ONR Atlantic Natural Laboratory, Mid-Atlantic Ridge, faults, scarp denudation, geophysical survey, multi-beam bathymetry	36
	16. PRICE CODE

17. SECURITY CLASSIFICATION OF REPORT	18. SECURITY CLASSIFICATION OF THIS PAGE	19. SECURITY CLASSIFICATION OF ABSTRACT	20. LIMITATION OF ABSTRACT
Unclassified	Unclassified	Unclassified	

DISCLAIMER NOTICE

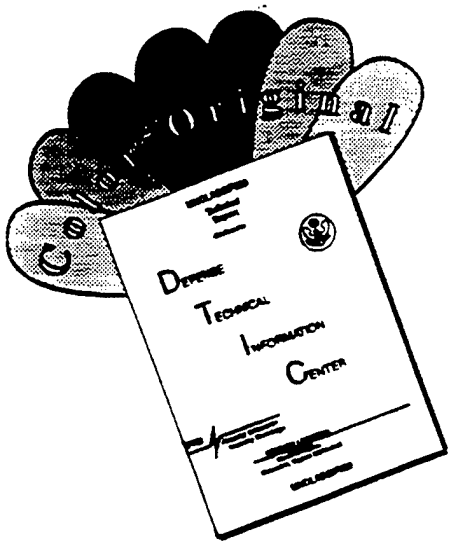

THIS DOCUMENT IS BEST QUALITY AVAILABLE. THE COPY FURNISHED TO DTIC CONTAINED A SIGNIFICANT NUMBER OF COLOR PAGES WHICH DO NOT REPRODUCE LEGIBLY ON BLACK AND WHITE MICROFICHE.

FINE-SCALE RECORD OF FAULTING IN ONR NATURAL LABORATORIES

Final Report for ONR Grant N00014-94-1-0466

Brian E. Tucholke, Gary E. Jaroslow and W. Kenneth Stewart
Woods Hole Oceanographic Institution, Woods Hole, MA 02543
Email: btucholke@whoi.edu, gjaroslow@whoi.edu, kstewart@whoi.edu
Ph. (508) 457-2994, (508) 457-2491, (508) 457-2644
FAX (508) 457-2187, (508) 457-2187, (508) 457-2191

Martin C. Kleinrock
Vanderbilt University, Nashville, TN 37235
Email: kleinrmc@ctrvax.vanderbilt.edu
Ph. (615) 322-2420
Fax (615) 322-2138

LONG-TERM GOALS

Our long-term goals are to understand the structure and evolution of ocean crust and its sedimentary load, and to develop models that successfully predict the character and variability of these features across multiple scales and in unsurveyed or poorly surveyed areas of the ocean basins. Our studies focus on 1) delineating the nature, magnitude, and relative importance of primary tectonic and magmatic processes that control formation of basement structure, 2) understanding secondary tectonic and sedimentary processes that modify the geologic record, 3) developing analytical tools to enhance interpretation of remotely sensed geological/geophysical data, and 4) formulating combined models of tectonism, magmatism, crustal aging and sedimentation that predict seafloor structure for slow-spreading ocean crust. Our investigations include the acoustic properties and morphotectonic structure of both the oceanic crust and its sedimentary record. The scales of interest for these properties range from sub-meter to hundreds of kilometers.

SCIENTIFIC AND TECHNOLOGICAL OBJECTIVES

In this project, our scientific objectives were 1) to characterize the fine-scale record of faulting and associated crustal structure in slow-spreading ocean crust, 2) to use this data to test and improve existing models of crustal structure, and 3) to address fundamental questions about the strength profile and deformation processes in young oceanic lithosphere. Our technological objectives were to develop quantitative analytical techniques which could be applied objectively to geophysical data to assist in resolution of the scientific problems of interest.

BACKGROUND AND APPROACH

In 1992 we acquired a detailed suite of geological/geophysical data over 0-29 m.y.-old crust on the Mid-Atlantic Ridge within the ONR Atlantic Natural Laboratory (Figures 1 and 2; Tucholke et al., in press, a). The survey was at 25°25' - 27°10'N, 45°00' - 49°00'W, and it constituted the Acoustic Reverberation Corridor for ONR's Acoustic Reverberation Special Research Program. Given that prior Mid-Atlantic Ridge studies focused near the spreading axis, this survey was a major step toward investigating the full spatial and temporal record of crustal accretion, tectonism, sedimentation and mass-wasting for slow-spreading ocean crust. In particular, an excellent suite of Hydrosweep multibeam bathymetric data and HMR1 sidescan-sonar data provided remarkably complete information about the distribution and character of faulting within Mid-Atlantic Ridge spreading segments. We analyzed these data both through conventional geologic interpretation and through newly developed quantitative analytical techniques. Our interpretations were ground-truthed by concurrent analysis of near-bottom, fine-scale survey data which we acquired in the Acoustic Reverberation Corridor in 1993.

RESULTS

Fault Analysis on the Mid-Atlantic Ridge Flank

Analytical Techniques for Fault Identification and Parameter Extraction

We initially concentrated on neighborhood texture analysis of HMR1 sidescan-sonar data within high-slope zones of ocean crust. Using supervised classification techniques, we derived feature vectors that successfully segmented out and identified fault-scarp zones (Figure 3; Tang and Stewart, 1994). Detailed near-bottom submersible and ROV observations previously showed that fault zones often consist of combinations of steeply dipping faults and interspersed low-dip features such as terraces and talus slopes. To assess whether such smaller-scale features could be differentiated in the HMR1 data, we selected a representative series of fault zones, made geological interpretations of likely fault-scarp and talus regions from combined multibeam bathymetric and sidescan-sonar data, and conducted supervised classification and neighborhood texture analysis of the sonar data in these regions. The results showed that the feature vectors are only partially successful in discriminating likely scarps from likely talus zones (Figure 3).

At least two factors that limit the application of this technique. First, while the HMR1 data have a nominal pixel size of 5 meters, the data are noisy at this scale and it is impractical to conduct texture analysis on 5-m data; the minimum practical cell size for analysis was determined to be about 25 meters. The minimum size of the neighborhood required for realistic textural analysis is 16x16 cells and robust analysis requires 32x32

cells. Because the fault zones which were being analyzed typically have a width of only a few hundred meters, the analysis is marginally at the limit of the technique and does not produce results with sufficient resolution to distinguish features of interest.

Perhaps more importantly, we found that the assumption of scarp and talus-ramp geometry probably is a gross oversimplification of true fault-zone character in most environments. We used the fine-scale, near-bottom survey data to ground-truth the geological character of selected fault scarps within the study area, and we found that the original scarps become massively dissected by slope failure and mass wasting (see Figures 14 and 15, and later summary). The scarp degradation begins near the Mid-Atlantic Ridge axis and actively continues to at least 10-20 m.y. off-axis. Slope modification previously had been observed by submersible and ROV studies near the ridge axis, but because of the very limited extent of these observations, the ultimate magnitude of the modifications had never before been appreciated. The scale of dissection ranges from 10's to 100's of meters, imparting strong geological variability at the typical scale of our neighborhood textural analyses. Thus, while the textural analyses of HMR1 sidescan data are successful in distinguishing fault zones per se, they are unlikely to differentiate consistently among sub-provinces within the fault-zone regions.

We also evaluated the consistency of correlation between fault zones extracted from HMR1 sidescan-sonar data and high-slope zones extracted from slope analysis of coincident Hydrosweep multibeam bathymetric data. Not unexpectedly, there is strong correspondence, and we consequently used the multibeam bathymetry for further analysis of fault characteristics. The advantages of using the bathymetry are: 1) computational efficiency in using this numerically smaller gridded data set, and 2) elimination of artificial "fault zones" that sidescan textural analysis can spuriously identify from local noise or at edges caused by gain differences in adjacent records.

Using multibeam bathymetry, we developed and applied semi-automated fault-detection and measurement techniques to quantitatively study the brittle strain taken up by faults (Jaroslow, 1997; Jaroslow and Tucholke, in prep.). The technique is based on image processing of rasterized bathymetry. First, "edges" were automatically detected in a digital raster image of bathymetry using gradient-based, edge-detecting software. This located individual points which group to form "edges" along the trace of high-dip zones (faults) on the seafloor; it also provided dip orientation. All detected edges were then visually compared to HMR1 sidescan-sonar images to identify and discard those edges that were interpreted from geological criteria not to represent faults. We also confirmed our interpretations of fault scarps in three locations using the high-resolution, near-bottom bathymetric and sidescan surveys from our 1993 cruise. Finally, for those edges identified

as faults, fault parameters were derived from the original, gridded multibeam bathymetric data. Processing and analysis steps were as follows:

1. Multibeam bathymetry was converted to a raster image of pixel intensity, where intensity was directly proportional to seafloor depth. Data gaps were filled with interpolated values, and resolution of the raster image was kept the same as that of the gridded bathymetry (1 pixel ≈ 200 m).

2. Edges (steepest seafloor gradients) were located from the local maxima in the gradients of a Gaussian smoothed image. A Gaussian filter with a standard deviation of 2 (determined by trial and error) was applied to control the balance between noise and the edges of interest (i.e., faults). Gradients were then calculated for each pixel, and all local maxima above a certain threshold were marked as an edge. The threshold was set to 4 degrees to reduce noise and optimize the signal of linear, continuous edges. A minimum edge-length of 8 pixels (1600 m) was also applied. This eliminated features too small and discontinuous to be considered faults. Examples of detected edges prior to interpretation are shown in Figure 4.

3. Detected edges were visually compared to HMR1-sidescan-sonar images to identify edges that represent faults and to eliminate non-fault edges. We applied two criteria to distinguish faults. First, following the technique of Laughton and Searle (1979), strong narrow sidescan echoes were interpreted as fault scarps and wider zones of more diffuse echoes were interpreted as rough, unfaulted volcanic terrain. Second, detected edges were considered to be faults only if they matched with continuous and generally linear sidescan echoes.

4. Edges identified as normal faults were analyzed using the original, 200-m gridded bathymetry to determine fault parameters for each detected point along the fault. Fault throw, apparent dip, and apparent heave were first measured in the local direction of maximum dip at 200 m intervals along the strike of the fault. As shown in Figure 5, throw and apparent fault dip were measured directly from bathymetry, and heave was calculated using these parameters. Fault throw was determined from the difference between maximum and minimum bathymetric depths in the local (apparent) dip direction, within a calculated range between faults (Figure 5); the calculated range is half the distance from the edge point of interest to the next closest edge point in the dip direction. Apparent dip was determined from the maximum depth gradient at the local edge point of interest. Apparent heave, h, was calculated as:

$$h = T \cdot \arctan(d),$$

where T = throw and d = apparent dip.

Once apparent heaves and dips were determined, they were geometrically corrected to "true" heave (H) and dip (D) by projecting them onto a line parallel to the average spreading direction in the study area (105°). Only "true" heave and dip were used in our subsequent analyses. Fault throws (T) were used as measured because they remain essentially constant regardless of dip direction.

Strain measurements were computed as area strain:

$$\varepsilon = \Delta A / A_0,$$

where ε = area strain, ΔA = change in the area of interest, and A_0 = initial area. The change in area, ΔA, was taken as the total plan-view seafloor expression of all faults lying within an area of interest; it was calculated from the summation of fault heaves of all individual fault points within that area, multiplied by the grid length of each point:

$$\Delta A = \Sigma (H \cdot l_g),$$

where H = fault heave of a point and l_g = point grid length (200 m). It follows that

$$A_0 = A - \Delta A,$$

where A = total area of the seafloor in the area of interest.

Changes in finite strain from area to area may reflect variation in the number of faults, the length of faults, and/or variations in incremental strain along individual faults. To assess the cause of changes in finite strain from area to area, we calculated total fault length (L), fault density (length normalized to area, L/A), and fault heave (H) for different areas within the study region. We used L because it combines the number of faults and their lengths into a single parameter by which to compare changes. By normalizing L by A, we can determine whether strain changes proportionately with fault density.

Spacing between faults was also measured along lines parallel to the average spreading direction (105°). We made measurements along 6 equidistant lines in each spreading segment so that the full along-isochron lengths of segments were represented.

To compare faulting at segment centers and ends, segments were divided into three equally spaced regions that roughly correspond to intrasegment tectonic settings. The middle third of each segment was treated as segment-center crust, and the outer thirds were treated as inside- or outside-corner crust, depending on the sense of offset in the non-transform discontinuity at the segment edge. This method of defining tectonic provinces by along-isochron, intrasegment distance is a simple approximation; it allowed first-order variations in fault populations to be compared among the three tectonic settings and avoided the subjectivity that would be involved in detailed interpretation of the complex boundaries between the tectonic settings.

Results of Fault Analysis

We applied the fault detection and measurement techniques to multibeam bathymetry over 0 - 20 Ma crust in three spreading segments (E, G, H; Figure 2), all bounded by non-transform discontinuities, within the Acoustic Reverberation Corridor. We studied both the temporal variability of faulting across isochrons and the spatial variability within segments (i.e., inside-corner, segment-center, and outside-corner crust). These analyses provided major new constraints on the role of faulting in the formation of topography at slow-spreading ridges (Jaroslow, 1997; Jaroslow and Tucholke, in prep.), and we here summarize the principal results.

Regionally, the calculated brittle strain taken up by faults is 30%. This is a maximum value because it does not account for two factors that may cause overestimation in our calculated heaves: a) bathymetric smoothing introduced by the large footprint (200 m) in the gridded multibeam data set, and b) the possibility that the individual "faults" we analyzed are actually fault zones consisting of several faults that dip at higher angles, so that the measurements that we made on a "fault" provide a composite result. Nonetheless, our measurements were made in a consistent way throughout the study area, and they are valid for examining internal spatial and temporal variations in faulting within this area. Slope degradation and sedimentation also might be expected to affect calculated heaves, but as will be shown later, this proved not to be a problem in our analyses.

If, instead of using measured fault dip, we assume that the faults dip at 45° (as has commonly been done in other studies of faulting at mid-ocean ridges), the total brittle strain calculated for our study area is reduced to 6%. This value is somewhat below values of 10-20% that have been proposed previously based on global estimates of seismic strain (Solomon et al., 1988) and local, near-bottom surveys in the rift-valley wall (e.g., Macdonald and Luyendyk, 1977).

A major finding of our study is that the form of the Mid-Atlantic Ridge rift valley is controlled by faulting on both inward-facing and outward-facing normal faults. Outward-facing faults account for 40% of the faults observed on the ridge flank (Figure 6). Measured strain on inward-facing faults decreases with crustal age in the rift-valley wall, while at the same time measured strain on outward-facing faults increases (Figure 7). Strain slowly decreases beyond the crest of the rift mountains, indicating that there is no active faulting on the ridge flank beyond 3-4 m.y. off-axis.

We explain the observed strain on inward- and outward-facing faults within the rift-valley wall in the following way. Uplift of crust from the rift-valley floor to the crest of the rift mountains is accommodated by extension on inward-facing normal faults; slip on these faults is concentrated near the base of the rift-valley walls, primarily in the major bounding

faults at the margins of the rift-valley floor, and these faults become inactive higher in the rift-valley walls. Fault-scarp erosion and sediment accumulation decrease the length (L) and fault density (L/A) of these inactive faults (Figure 8, left), and thus they also decrease fault strain (ε) because fault heave is constant (Figure 7, see discussion of heave below). Outward-facing faults form in the middle to upper parts of the rift-valley walls, and slip on these faults reduces and eventually eliminates rift-valley relief as crust reaches the crest of the rift mountains. Because these faults are actively growing, L and L/A (and thus ε) increase faster than they are reduced by scarp erosion and sedimentation (Figure 8, right).

Interestingly, fault heave is essentially constant from the lower rift-valley walls onto the ridge flank (Figure 7). This seems paradoxical because scarp erosion should decrease measured fault dip over time and thus increase calculated fault heave. We find, however, that as scarp dip is decreased, fault throw is decreased proportionately (Figure 9), with the result that calculated heave is relatively invariant, despite the fact that fault scarps actually are degrading with time.

Both inward- and outward-facing faults are responsible for the creation of abyssal-hill topography. Inward- and outward-facing faults commonly appear in pairs (Figure 6), and they consequently create horst and graben terrain that forms most abyssal hills (e.g., Figure 10). The remaining abyssal hills are formed largely by single inward- or outward-facing faults that create half-graben.

Regionally, high fault density and high fault strain correlate with increased residual mantle Bouguer anomaly (i.e., thin crust) that is attributable to relatively amagmatic extension at the ridge axis. Similarly, low fault densities and low strains correlate with reduced residual mantle Bouguer anomaly (thicker crust) that is attributable to more magmatic extension. Thus we find that there is a negative correlation between brittle strain and robustness of magmatic accretion at the ridge axis.

We also found that the percentage of outward-facing faults, based on total fault length, consistently increases with increasing residual mantle Bouguer anomaly, and in regions of high values ($\geq$15 mGal) it is approximately double that in regions of low values ($\leq$7 mGal). From this and our other observations of fault patterns, we developed a model that relates the formation of outward-facing faults to the development of a decoupling horizon near the base of the crust, caused by near-axis formation of serpentinites (Figure 11). This decoupling zone, together with rotation of the axis of maximum principal compressive stress associated with lithosphere necking (Tapponnier and Francheteau, 1978), favors the formation of outward-facing faults in the upper rift-valley walls. The great advantage of this model is that it overcomes the problem, evident in conventional isotherm-based models

(Carbotte and Macdonald, 1990), that outward-facing faults would have to cut through thicker lithosphere than inward-facing faults.

Observed fault strain on the rift flank beyond the crest of the rift mountains slowly decreases with age (Figure 7). We attribute this to long-term degradation of fault scarps and burial by sediments, both of which tend to reduce L and L/A, and thus ε, given that heave is relatively constant. Short-term (~3 m.y.) temporal variations in brittle strain also are observed on the ridge flank (Figure 7). These appear to reflect variability in magmatic versus relatively amagmatic extension at the ridge axis.

Finally, we studied changes in fault parameters within individual spreading segments, and we found that fault populations show strong differences in geometry, density and strain with intrasegment tectonic setting. Observations on inside-corner crust are consistent with faulting of relatively thick, cold lithosphere with limited magmatic extension; strains are large and fault spacings tend to be greater than those at segment centers. At segment centers, faults are longer, more linear, more closely spaced, and have smaller offsets and lower strains; this pattern suggests a thinner brittle lid and more magmatic extension. Comparison of brittle strain between individual ridge segments also suggests that strain near segment ends is enhanced as the magnitude of offset increases at the non-transform discontinuities between the segments.

Quantitative Analysis of Abyssal Hills

The multibeam bathymetry acquired during Ewing Cruise 9208 also presented a first opportunity to do an extensive statistical analysis of abyssal-hill morphology on a slow-spreading ridge, and we investigated the relationship between the abyssal hills and the properties of the ridge axis at which they were formed (Goff et al., 1995). We applied the Goff-Jordan (1988) method to estimate two-dimensional statistical properties of abyssal-hill morphology in three spreading segments (E, G, H; Figure 2), deriving root-mean-square (rms) height, characteristic width, and plan-view aspect ratio. The study was done in two parts: 1) analysis of near-axis (<7 Ma) abyssal hills for each of the three segments, and 2) analysis of temporal variations (2-29 m.y. off-axis) in abyssal-hill morphology along the run of the southernmost segment. In this study the results of our analysis also were compared with the residual mantle Bouguer gravity data and with an early determination of fault characteristics based HMR1 sidescan-sonar data. Our findings were consistent with the results of the more detailed fault study described in the previous section.

We found that abyssal-hill morphology is strongly related to tectonic setting (i.e., inside corner vs. outside corner) within a segment. Abyssal hills forming at inside corners have larger rms height and characteristic width and smaller plan-view aspect ratio than

those originating at outside corners. We also found that along-flow-line variations in rms height and characteristic width are positively correlated with residual mantle Bouguer gravity anomaly but plan-view aspect ratio is negatively correlated.

Comparison between segments of differences in abyssal-hill morphology and differences in residual mantle Bouguer gravity anomaly shows the same kind of relationships. From these results, we infer that lower-relief, narrower, and more elongated abyssal hills are produced when thicker crust is being generated. We also made an intersegment comparison of variations in near-axis rms height and average fault density (as determined from analysis of HMR1 sidescan-sonar imagery), and we found that rms height and fault density correlate negatively with one another.

Fast-Propagating Rifts in Slow-Spreading Crust

Within the spreading segments identified in the study area, we found a number of highly oblique fault zones that cut across the full segment length between bounding non-transform discontinuities (Tucholke et al., 1995; Kleinrock et al., submitted). The best developed of these structures are a pair of features which appear in ca. 11 Ma and 15 Ma crust within the robust, long-lived segment E (bold dashed lines, Figure 2). Through time, the structures cut progressively from north to south across the segment, but they did not significantly alter its overall length or integrity. Each structure is characterized by a pronounced morphological depression, by truncation of normal abyssal hills, and by a right-lateral offset of magnetic anomalies. We interpreted these structures to have been formed by rapid southward propagation of small (5-7 km), right-lateral offsets of the rift axis. They developed in crust with a spreading half-rate of 14-15 km/m.y., and they propagated at a rate of 25-30 km/m.y.

For such southward propagation and right-lateral anomaly offset, each observed trace on the western flank of the Mid-Atlantic Ridge represents an inner pseudofault (IPF) zone, a region of sheared lithosphere transferred from the African to the North American plate. The IPFs have distinct gravity signatures; they mark a relatively rapid transition from a reduced residual mantle Bouguer anomaly in older crust to an elevated anomaly in younger crust, thus suggesting a change from thicker to thinner crust. We interpreted the propagation of each of these small discontinuities to have been triggered by the onset of an episode of relatively amagmatic extension.

The other propagators within the survey region have the same essential features, including IPF tectonic setting, but they are not as well developed. All observed propagators migrated southward. However, it is difficult to distinguish subtle magnetic-anomaly perturbations at outer pseudofaults of possible northward-propagating rifts in this

slow-spreading environment, so this observation may be an artifact rather than an indicator of preferred direction of propagation.

Degradation and Destruction of Seamounts by Faulting

In a study funded separately by ONR, we identified 86 axial seamounts and 1290 off-axis seamounts (near-circular volcanoes) that are ≥ 60 m high within the study area out to ~29 Ma crust (Figure 12; Jaroslow et al., 1994, 1995, 1996; Jaroslow, 1997). From our analyses, we interpreted the seamounts to have formed on the inner rift-valley floor of the Mid-Atlantic Ridge; thus the seamounts and seamount remnants on the ridge flank are important to interpreting how crust is faulted as it is transported out of the rift valley.

The abundance of off-axis seamounts demonstrates that large sections of ocean crust are carried intact from the rift-valley floor through the rift-valley walls and onto >4 Ma crust on the ridge flank. However, there are significant changes in seamount population density, size distribution, and shape between ridge axis and ridge flank, and these are caused by faulting between ~0.6 and 3-4 m.y. off-axis in the rift-valley walls (Figure 13). During initial transport of seamounts from the rift valley (0.6 - 2 m.y.), few seamounts are destroyed by the inward-facing faults, but seamount height is significantly decreased. In the upper portions of the rift-valley wall, on 2 - 4 Ma crust, additional faults (outward-facing) destroy and degrade a significant number of seamounts. These results are consistent with evidence, noted earlier, that outward-facing faults appear in the upper portions of the rift-valley walls.

Beyond the crest of the rift mountains (>4 Ma), faulting is no longer active, and changes in the off-axis seamount population probably reflect long-period crustal aging processes and temporal changes in seamount production that occurred at the ridge axis. A marked increase in seamount population density occurs on ~20 - 24 Ma crust; although it may have been caused by an increase in axial seamount production at that time, it is also possible that it reflects a decrease in seamount destruction that is related to reduced density of faults.

Fine-Scale Studies of Faults on the Mid-Atlantic Ridge Flank

We conducted detailed near-bottom, high-resolution surveys of fault scarps on Knorr Cruise 138-14 in 1993 (Kleinrock and Tucholke, 1993; Shaw et al., 1993; Tucholke et al., 1993). As part of our subsequent fault studies, we analyzed near-bottom survey data from three sites in the Acoustic Reverberation Corridor. All sites were adjacent to the non-transform discontinuity between segments E and G on the ridge flank. Site D was on ~4 Ma inside-corner crust, Site A was on ~11 Ma outside-corner crust, and Site B was on ~24

Ma segment-center to outside-corner crust. Data collected at these sites included sidescan backscatter amplitude and phase-difference bathymetry (120 kHz, 200 kHz); forward-scan sonar (300 kHz); precision pencil-beam bathymetry; magnetics; video, film, and electronic still photography; and seafloor rock samples.

The near-bottom surveys showed steeply dipping scarps (40°-90°, locally overhanging) that vary in height from a few tens of meters to more than 200 m, separated by relatively low-slope to level, sediment-covered ponds and terraces. Moderate-slope (20°-40°) talus ramps lie at the bases of scarps. The scarps typically exhibit truncated pillow-basalt structures or show slab-like faces that may be zones of fault gouge.

Although the scarps were formed originally by faulting, they have been strongly altered by mass wasting and erosion. Our near-bottom surveys provided unique new insights into the processes and products of denudation, and they showed that fault scarps can be significantly denuded for periods up to 10-20 m.y. or more (Tucholke et al., 1994; in press, a).

The principal mechanism of denudation appears to be mass wasting (gravitational failure), including slumps and slides at scales up to 1 km or more. Debris flows and turbidity currents probably form by disaggregation of small failed blocks, and they may contribute significantly to erosion of canyons and gullies through abrasion. Scarp failure is thought to be facilitated largely by intracrustal weathering in pre-existing zones of weakness such as faults, fissures, and flow contacts. Seismic shock probably is important in triggering failure within the seismically active rift valley (≤2 Ma), but it becomes less effective with distance onto the relatively aseismic ridge flank.

Initial denudation forms cross-scarp chutes and gullies. With time, these develop into canyons that cut progressively deeper into scarps and are joined by scarp-parallel gullies to create trellis drainage patterns (Figures 14, 15). This process continues out to crust at least 24 m.y. old, although the rate of denudation probably diminishes with time as average scarp dips decrease. In mature trellis drainage, resistant ridges commonly are reduced to sharp-edged, arete-like form by lateral denudation in the walls of adjacent canyons and gullies. Development of trellis patterns appears to result from excision of rock in structurally weak zones, i.e., along faults and fractures that formed in a roughly rectilinear pattern near the ridge axis and that were subjected to intracrustal weathering. The long temporal record of scarp failure suggests that exposed scarps are not significantly stabilized off-axis by secondary mineralization and sealing in the weak zones. Canyon-cutting into exposed scarps proceeds at average rates of 10-20 m/m.y. The steepest dips along original scarp faces are reduced from >50° on 4 Ma crust to 35°-40° on 24 Ma crust, and scarp widths markedly increase.

These changes in morphology and slope are important to consider in interpretations of crustal tectonics. As noted earlier, within our study area decreases in fault dip caused by scarp degradation appear to be complemented by decreases in fault throw (Figure 9), resulting in relatively constant heave. However, this may not hold true in other areas. If heave is computed from apparent fault dips of degraded scarps rather than from reconstruction of true dips, and concomitant changes in fault throw are not documented or are not properly accounted for, derived strain could be strongly mis-estimated.

Multi-Scale Spectral Analysis of Seafloor Bathymetry

We also used Hydrosweep multibeam bathymetry from the study area, together with Mesotech scanning pencil-beam bathymetry derived from the near-bottom surveys, to conduct a multi-scale spectral analysis of topography (Goff and Tucholke, in press). These data were compared with visual data from the near-bottom surveys, which enabled us to identify bathymetric profiles that are on unsedimented or thinly sedimented crust. Our analysis thus focused primarily on statistical characterization of basement morphology. We concentrated on two sites: Site B on ~24 Ma crust in a segment-center to outside-corner tectonic setting, and Site D on ~4 Ma crust in an inside-corner setting.

At Site B we found that an anisotropic, band-limited fractal model (i.e., the "von Kármán" model of abyssal hill morphology) is not sufficient to describe the full range of scales observed. Our observations differ from the von Kármán model in two ways: 1) strike and cross-strike (dip) spectral properties converge for wavelengths smaller than ~300m, and 2) in both strike and dip directions the fractal dimension changes at ~10 m wavelength, from ~1.27 at larger scales to ~1.0 at smaller scales. The convergence of strike and dip spectral properties appears to be associated with destruction of the ridge-parallel fault scarps by mass wasting, which develops canyon-like incisions that cross scarps at high angles (Figure 14). The change in fractal dimension at ~10 m scale appears to be related to a minimum spacing of significant slope breaks associated with scarps which are created by faulting and mass wasting.

At Site D there is no significant abyssal-hill anisotropy, but the spectral properties at all scales are consistent with the von Kármán model. The fractal dimension at this site (~1.15) is less than at Site B. This difference may reflect different morphology related to formation of crust in an inside- versus outside-corner tectonic setting or, more likely, it reflects differences in the degree of mass wasting in the young (~4 Ma) crust of Site D versus the old crust (~24 Ma) at Site B. In general, smoothing of seafloor morphology by sediments is evident in Hydrosweep periodograms where, relative to basement roughness, spectral power decreases progressively with decreasing wavelength.

SCIENTIFIC IMPACT AND TRANSITIONS

The quality and spatial/temporal coverage of the data which we studied are unique in the ocean basins. These data provide major new insights into how brittle strain is partitioned according to intrasegment tectonic setting and variation in magma input at the rift axis. They provide the first solid documentation of how patterns of normal faulting account for the shape of the rift valley in slow-spreading crust, and they clearly show that typical abyssal-hill morphology is fault-controlled. Finally, the fine-scale data demonstrate for the first time the remarkable, long-term denudation experienced by fault scarps in igneous ocean crust. The analytical techniques that we developed and tested will be widely applicable to analysis of sonar data from all ocean environments. The insights into basement roughness and backscatter patterns from ocean crust gained from this study also directly benefitted efforts to understand acoustic reverberation from the ocean bottom and subbottom within ONR's Acoustic Reverberation Special Research Program.

REFERENCES CITED

Carbotte, S.M., and K.C. Macdonald, Causes of variation in fault-facing direction on the ocean floor, Geology, v. 18, p. 749-752, 1990.

Goff, J.A., and T.H. Jordan, Stochastic modeling of seafloor morphology: Inversion of Sea Beam data for second-order statistics, J. Geophys. Res., v. 93, p. 13,589-13,608, 1988.

Goff, J.A., B.E. Tucholke, J. Lin, G.E. Jaroslow, and M.C. Kleinrock, Quantitative analysis of abyssal hills in the Atlantic Ocean: A correlation between crustal thickness and extensional faulting, J. Geophys. Res., v. 100, p. 22,509-22,522, 1995.

Goff, J.A., and B.E. Tucholke, Multi-scaled spectral analysis of seafloor bathymetry on the flanks of the Mid-Atlantic Ridge, J. Geophys. Res. (in press).

Jaroslow, G.E., The Geological Record of Oceanic Crustal Accretion and Tectonism at Slow-Spreading Ridges, Ph.D. Thesis, Massachusetts Institute of Technology - Woods Hole Oceanographic Institution Joint Program in Oceanography, 210 pp., 1997.

Jaroslow, G.E., D.K. Smith, and B.E. Tucholke, The off-axis record of volcanism in the western North Atlantic Ocean, EOS Trans. Am. Geophys. Union, v. 75, no. 44 (Fall Meeting Supplement), p. 660, 1994.

Jaroslow, G.E., D.K. Smith, and B.E. Tucholke, Production and evolution of seamounts in the ONR Natural Laboratory, North Atlantic Ocean, EOS Trans. Am. Geophys. Union, v. 76, no. 46 (Fall Meeting Supplement), p. F553-F554, 1995.

Jaroslow, G.E., D.K. Smith, and B.E. Tucholke, Seamount production and evolution in the western North Atlantic Ocean, 25°30' - 27°10'N: FARA-InterRidge Mid-Atlantic Ridge Symposium, 19-22 June 1996, Reykjavik, Iceland, Journal of Conference Abstracts, v. 1, p. 802, 1996.

Kleinrock, M.C., and B.E. Tucholke, Evidence from towed and remotely operated vehicles for variations in the structure of the traces of nontransform offsets at the Mid-Atlantic Ridge, EOS Trans. Am. Geophys. Union, v. 74, no. 43, p. 574, 1993.

Kleinrock, M.C., B.E. Tucholke, J. Lin, and M.A. Tivey, Fast rift propagation at a slow-spreading ridge: Progressive tearing of an entire spreading segment, Geology (submitted).

Laughton, A.S., and R.C. Searle, Tectonic processes on slow spreading ridges, *In:* M. Talwani, C.G. Harrison, & D.E. Hayes (Eds.), *Deep Drilling Results in the Atlantic Ocean: Ocean Crust.* Am. Geophys. Union, M. Ewing Series, v. 2, p. 15-32, 1979.

Macdonald, K.C., and B.P. Luyendyk, Deep-tow studies of the structure of the Mid-Atlantic Ridge crest near lat 37°N, Geol. Soc. Am. Bull., v. 88, p. 621-636, 1977.

Shaw, P.R., M.C. Kleinrock, and B.E. Tucholke, Multiscale analysis of the tectonic fabric of the northern Mid-Atlantic Ridge flank, EOS Trans. Am. Geophys. Union, v. 74, no. 43, p. 574, 1993.

Solomon, S.C., P.Y. Huang, and L. Meinke, The seismic moment budget of slowly spreading ridges, Nature, v. 334, p. 469-481, 1988.

Tang, X., and W.K. Stewart, Texture analysis using principal component analysis techniques, *In:* Proceedings of the SPIE Conference on Image and Signal Processing for Remote Sensing, v. 2315, p. 22-35, 1994.

Tapponnier, P., and J. Francheteau, Necking of the lithosphere and the mechanics of slowly accreting plate boundaries, J. Geophys. Res., v. 83, p. 3955-3870, 1978.

Tucholke, B.E., M. Kleinrock, and W.K. Stewart, Fine-scale, near-bottom surveys of ocean crust on the flank of the Mid-Atlantic Ridge, 26 to 27 degrees North, EOS Trans. Am. Geophys. Union, v. 74, no. 43, p. 574, 1993.

Tucholke, B.E., W.K. Stewart, and M.C. Kleinrock, Dissection and degeneration of fault scarps observed by fine-scale survey of slow-spreading ocean crust, EOS Trans. Am. Geophys. Union, v. 75, no. 44 (Fall Meeting Supplement), p. 649, 1994.

Tucholke, B.E., M.C. Kleinrock, M. Tivey, and J. Lin, Fast-propagating rifts in slow-spreading crust, EOS Trans. Am. Geophys. Union, v. 76, no. 46 (Fall Meeting Supplement), p. F554, 1995.

Tucholke, B.E., J. Lin, M.C. Kleinrock, M. Tivey, T.B. Reed, J. Goff, and J. Jaroslow, Segmentation and crustal structure of the western Mid-Atlantic Ridge flank, 25°30' - 27°10' and 0 - 29 m.y., J. Geophys. Res. (in press, a).

Tucholke, B.E., W.K. Stewart, and M.C. Kleinrock, Long-term denudation of ocean crust in the central North Atlantic Ocean, Geology (in press, b).

BIBLIOGRAPHY OF RESEARCH SUPPORTED BY THIS GRANT

Research Papers in Scientific Journals

Goff, J.A., B.E. Tucholke, J. Lin, G.E. Jaroslow, and M.C. Kleinrock, Quantitative analysis of abyssal hills in the Atlantic Ocean: A correlation between crustal thickness and extensional faulting, J. Geophys. Res., v. 100, p. 22,509-22,522, 1995.

Goff, J.A., and B.E. Tucholke, Multi-scaled spectral analysis of seafloor bathymetry on the flanks of the Mid-Atlantic Ridge, J. Geophys. Res. (in press).

Kleinrock, M.C., B.E. Tucholke, J. Lin, and M.A. Tivey, Fast rift propagation at a slow-spreading ridge: Progressive tearing of an entire spreading segment, Geology (submitted).

Robertsson, J.O.A., K. Holliger, A. Levander, J.A. Goff, H.F. Webb and B.E. Tucholke, A numerical analysis of ocean acoustic reverberation data from the proximity of the Mid-Atlantic Ridge, J. Acoust. Soc. America (submitted).

Tucholke, B.E., J. Lin, M.C. Kleinrock, M. Tivey, T.B. Reed, J. Goff, and J. Jaroslow, Segmentation and crustal structure of the western Mid-Atlantic Ridge flank, 25°30' - 27°10' and 0 - 29 m.y., J. Geophys. Res. (in press, a).

Tucholke, B.E., W.K. Stewart, and M.C. Kleinrock, Long-term denudation of ocean crust in the central North Atlantic Ocean, Geology (in press, b).

Ph.D. Theses

Jaroslow, G.E., The Geological Record of Oceanic Crustal Accretion and Tectonism at Slow-Spreading Ridges, Ph.D. Thesis, Massachusetts Institute of Technology - Woods Hole Oceanographic Institution Joint Program in Oceanography, 210 pp., 1997.

Abstracts

Jaroslow, G.E., D.K. Smith, and B.E. Tucholke, Production and evolution of seamounts in the ONR Natural Laboratory, North Atlantic Ocean, EOS Trans. Am. Geophys. Union, v. 76, no. 46 (Fall Meeting Supplement), p. F553-F554, 1995.

Jaroslow, G.E., D.K. Smith, and B.E. Tucholke, Seamount production and evolution in the western North Atlantic Ocean, 25°30' - 27°10'N: FARA-InterRidge Mid-Atlantic Ridge Symposium, 19-22 June 1996, Reykjavik, Iceland, Journal of Conference Abstracts, v. 1, p. 802, 1996.

Kleinrock, M.C., B.E. Tucholke, and J. Lin, Geometry and structure of inside corners and pseudofaults at a slow-spreading ridge, EOS Trans. Am. Geophys. Union, v. 77, no. 46 (Fall Meeting Supplement), p. F723, 1996.

Lin, J., B.E. Tucholke, M.C. Kleinrock, and J. Escartin, Contrasting inside- vs. outside-corner crustal structure on flanks of a slow-spreading ridge, EOS Trans. Am. Geophys. Union, v. 76, no. 46 (Fall Meeting Supplement), p. F554, 1995.

Lin, J., B.E. Tucholke, M.C. Kleinrock, and J. Escartin, Along- and across-isochron gravity and bathymetric anomalies on the Mid-Atlantic Ridge: Implications for tectonics of slow-spreading crust, EOS Trans. Am. Geophys. Union, v. 77, no. 46 (Fall Meeting Supplement), p. F724, 1996.

Shaw, P.R., M.A. Tivey, B.E. Tucholke, M.C. Kleinrock, and J. Lin, Past plate motions recorded in abyssal hill lineations and magnetic lineations on the western flank of the MAR, 26N, EOS Trans. Am. Geophys. Union, v. 75, no. 16 (Spring Meeting Supplement), p. 330, 1994.

Tucholke, B.E., W.K. Stewart, and M.C. Kleinrock, Dissection and degeneration of fault scarps observed by fine-scale survey of slow-spreading ocean crust, EOS Trans. Am. Geophys. Union, v. 75, no. 44 (Fall Meeting Supplement), p. 649, 1994.

Tucholke, B.E., M.C. Kleinrock, M. Tivey, and J. Lin, Fast-propagating rifts in slow-spreading crust, EOS Trans. Am. Geophys. Union, v. 76, no. 46 (Fall Meeting Supplement), p. F554, 1995.

Tucholke, B.E., J. Lin, and M.C. Kleinrock, Off-axis structure of spreading segments on the Mid-Atlantic Ridge flank near 26°N, ODP-InterRidge-IAVCEI Workshop, The Oceanic Lithosphere and Scientific Drilling into the 21st Century, 26-28 May 1996, North Falmouth, MA, p. 111, 1996.

Tucholke, B.E., Structure of mid-ocean ridges, NAGT Symposium, Plate Tectonics, What Students Should Know; Geol. Soc. Am. Abstr. with Programs, v. 28, no. 7, p. A-223, 1996.

Tucholke, B.E., J. Lin, and M. C. Kleinrock, Mullions, megamullions, and metamorphic core complexes on the Mid-Atlantic Ridge, EOS Trans. Am. Geophys. Union, v. 77, no. 46 (Fall Meeting Supplement), p. F724, 1996.

Abstracts of Presentations at ONR - ARSRP Research Symposia

Tucholke, B.E., W.K. Stewart, and M.C. Kleinrock, Irregularity of fault scarps in the Acoustic Reverberation Corridor caused by slope failure and mass wasting, Acoustic Reverberation Special Research Program, 1995 Research Symposium, 19-21 July 1995, Woods Hole Ocean. Inst., Woods Hole, MA, 1995.

FIGURE CAPTIONS

Figure 1 - Location of the ARSRP Acoustic Reverberation Corridor over 0-29 Ma crust on the west flank of the Mid-Atlantic Ridge. The Mid-Atlantic Ridge axis (double line) and off-axis traces of transform faults (labeled) and non-transform discontinuities (light lines) are interpreted from the marine gravity field derived from satellite altimetry. Other detailed surveys along the Mid-Atlantic Ridge extend ~10 m.y. off-axis (ATLANTIS, SARA, and SEADMA).

Figure 2 - Magnetic anomalies and tectonic interpretation of ridge-flank segments (identified by letters) in the Acoustic Reverberation Corridor. Magnetic anomalies are numbered, and crustal ages (Ma) are shown along the top of the figure in parentheses; fine lines locate positive anomalies and heavier lines locate negative (r) anomalies. Non-transform discontinuities, where identifiable in sea-floor morphology, are shown as black heavy lines at right-stepping offsets, as open lines at left-stepping offsets, and as dashed lines where weakly developed. The bold dashed lines in Segment E locate traces of two fast-propagating rifts. A major ~9° counterclockwise change in relative plate motion occurred following ~24 Ma (bold lines at left). Short dashes outline the limit of multibeam bathymetric coverage.

Figure 3 - East-dipping fault zones segmented into scarp or talus types using textural features (derived from supervised classification of sidescan sonar) as classification discriminants. The segmentation result here gives only 74% correct identification of the original classification template. Note that the size of texture neighborhoods (16x16) does not allow sufficient resolution for accurate results.

Figure 4 - Example of detected edges using image processing technique (described in text), superimposed on multibeam bathymetry (left), and on mosaicked HMR1 sidescan sonar images (center, right), prior to editing of processing artifacts and removal of non-fault edges. Each edge consists of individual data points spaced 200 m apart;. East-dipping edge points are identified by black or blue crosses and west-dipping points are red. This example site is located on ~7 Ma crust. Map coordinates are in Universal Transverse Mercator units; see Figure 5 for latitude and longitude.

Figure 5 - Example of the automated technique employed in measuring fault parameters. Fault throw and dip are measured directly from bathymetry and fault heave is geometrically derived. Map of multibeam bathymetry (top) is overlain by detected fault edges (black dots) The cross-section A-A', shown at bottom, is oriented in the

direction of maximum local dip (i.e., apparent dip) at point "X" along the fault edge. Vertical (throw) and horizontal (apparent heave) offset are calculated for each such point along the fault edge. Example site is the same as in Figure 4.

Figure 6 - Map of all inward-facing (blue) and outward-facing (red) normal faults identified in our fault study (0-20 Ma crust) within the Acoustic Reverberation Corridor. Segment boundaries are marked by gray lines, and the ridge axis is shown by heavy black lines. Thin black lines indicate crustal ages (Ma). The strike of most faults is parallel or subparallel to average plate-boundary orientation, marked by the arrow in the upper left corner. Note that pairs of closely spaced inward- and outward- facing faults are common, and they create elongate horsts that form most abyssal hills (e.g., Figure 10).

Figure 7 - Plots of fault parameters versus crustal age for the three ridge segments analyzed in this study. Arrows indicate the age of the crest of the rift mountains in each segment. Solid lines are totals for all faults, bold dashed lines are inward-facing faults, and thin dashed lines are outward-facing faults. Data are in 1 m.y. age bins. See text for description of fault parameters.

Figure 8 - Schematic illustration of how mass-wasting and sedimentation is thought to affect fault parameters for inactive (left) and actively growing faults (right) through time (t_1 to t_3) in the rift-valley walls. Gray shading indicates exposed, measurable fault surface. Unshaded regions indicate reduction in the measurable fault surface due to deposition of talus and sediments at the base of the fault scarp. H remains relatively constant with time because of reduction in both dip and throw (see Figure 9), but L and L/A (and thus ε) change significantly, as indicated.

Figure 9 - a) Plots of mean throws and dips versus crustal age for all faults in the three spreading segments studied. Values are for 1 m.y. age bins. b) Plot of mean throw versus dip (asterisks) for values in (a). Dashed lines represent the geometrical relationship between fault throw and dip needed to maintain constant heave, labeled in meters; solid line indicates the approximate constant mean heave for our study area. The plot suggests that the mean fault heaves, geometrically derived from measured fault throws and dips, may remain relatively constant even though scarp denudation causes throws and dips to decrease over time.

Figure 10 - Bathymetric map of a horst (ridge marked by arrow) formed by an inward-facing (east-dipping) and outward-facing (west-dipping) pair of faults (~ 6 Ma crust).

Such horsts commonly account for the form of abyssal hills on the ridge flank. Contour interval is 100 m.

Figure 11 - Schematic cross-sections of the Mid-Atlantic Ridge from the ridge axis (right) out to ~5.5 Ma crust (no vertical exaggeration) showing our geological model of faulting in the rift valley. Active faults are shown as solid lines and inactive faults are shown as dashed lines. Serpentinites are indicated by the hatched pattern. a) Model for thick crust formed during relatively magmatic extension. Few inward-facing faults reach the base of the crust in the lower rift-valley walls, so seawater rarely penetrates through the crust to facilitate serpentinization of the mantle; outward-facing faults thus form rarely and only in locations where serpentinites create a local, ductile layer at the base of the crust. b) Model for thin crust formed during relatively amagmatic extension. Inward-facing faults commonly extend through the crust and allow seawater penetration to the mantle; thus a ductile upper-mantle serpentinite layer is well developed. Outward-facing faults readily form in the thin, brittle crustal lid as lithospheric necking rotates the stress field in the rift-valley walls. In both a) and b), slip on faults in crust older than 3-4 Ma is very rare.

Figure 12 - Color bathymetric map of combined SeaBeam and Hydrosweep multibeam bathymetry in the Acoustic Reverberation Corridor, with identified seamounts shown as black dots; dot size is proportional to mean seamount diameter. Segment boundaries and the Mid-Atlantic Ridge axis are indicated by thin white lines.

Figure 13 - Schematic cross-section of the rift valley showing pattern of normal faulting on inward- and outward-facing faults (upper panel; see Figure 11), with plots of seamount parameters versus age (lower panels). Circled numbers in upper panel relate to local fault pattern, which is responsible for off-axis changes in seamount parameters: (1) the relatively unfaulted inner rift-valley floor, (2) the lower walls of the rift valley where faults are predominantly inward-facing, (3) the upper rift-valley wall to the crest of the rift mountains, where inward-facing faults become inactive and outward-facing faults develop, (4) the ridge flank where there are no active faults. The lower panels show estimated seamount density (ν_{ot}); characteristic height (β^{-1}); height-to-diameter ratio (ξ_d); and plan-view aspect ratio (D_{max}/D_{min}), versus crustal age/distance from the ridge axis. Errors of one standard deviation about the estimated parameter are shown on the y-axis.

Figure 14 - a) Three-dimensional perspective of DSL-120 bathymetry at Site B on ~24 Ma crust, illuminated from northeast. No vertical exaggeration. Note the three major east-dipping fault scarps that are heavily dissected by canyons, and the slide masses along the base of the central scarp. Strongly smoothed areas at the perimeter are regions for which there are no bathymetric data. Subtle horizontal "layering" along the central scarp is a data-processing artifact. b) Similar view of DSL-120 bathymetry at Site A on ~11 Ma crust. East-dipping fault scarps are more numerous and smaller than at Site B, and crosscutting canyons are less well developed.

Figure 15 - DSL-120 sidescan-sonar images of fault scarps (strong backscatter is dark) at Sites B, A, and D within the Acoustic Reverberation Corridor. a) East-dipping central scarp at Site B (see the upper panel of Figure 14) centered at 26°34.3'N, 48°04.6'W. The scarp is extensively dissected into a trellis pattern of cross-scarp canyons and intersecting scarp-parallel gullies. b) East-dipping scarp at eastern edge of Site A (see the lower panel of Figure 14) centered at 26°07.8'N, 46°12.2'W. A nascent trellis drainage pattern is observed. c) South-southeast-dipping scarp at Site D (~4 Ma crust) centered at 26°05.0'N, 45°15.8'W. Faults around displaced blocks probably will develop into cross-scarp canyons over time. Small scarp-parallel faults are visible but have not developed into gullies to form a trellis drainage pattern.

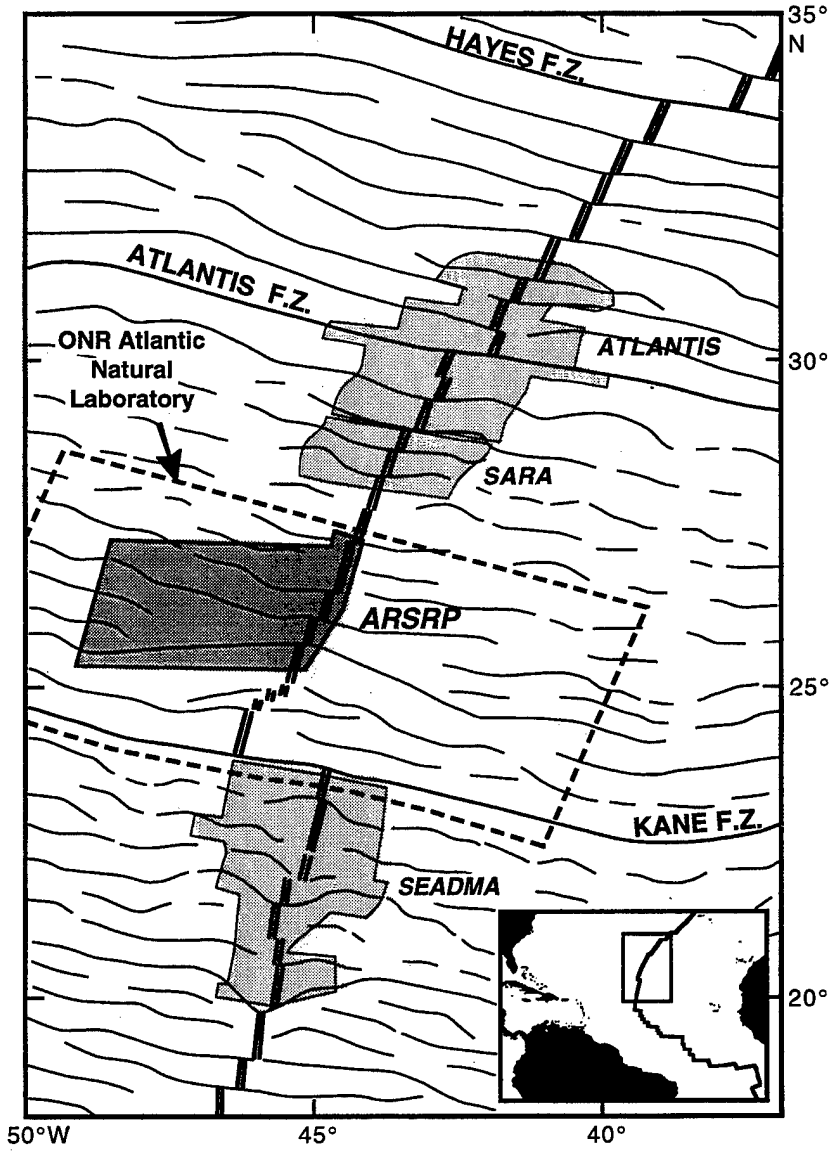
HAYES F.Z.
35° N
ATLANTIS F.Z.
ONR Atlantic Natural Laboratory
ATLANTIS
30°
SARA
ARSRP
25°
KANE F.Z.
SEADMA
20°
50°W
45°
40°

Figure 1

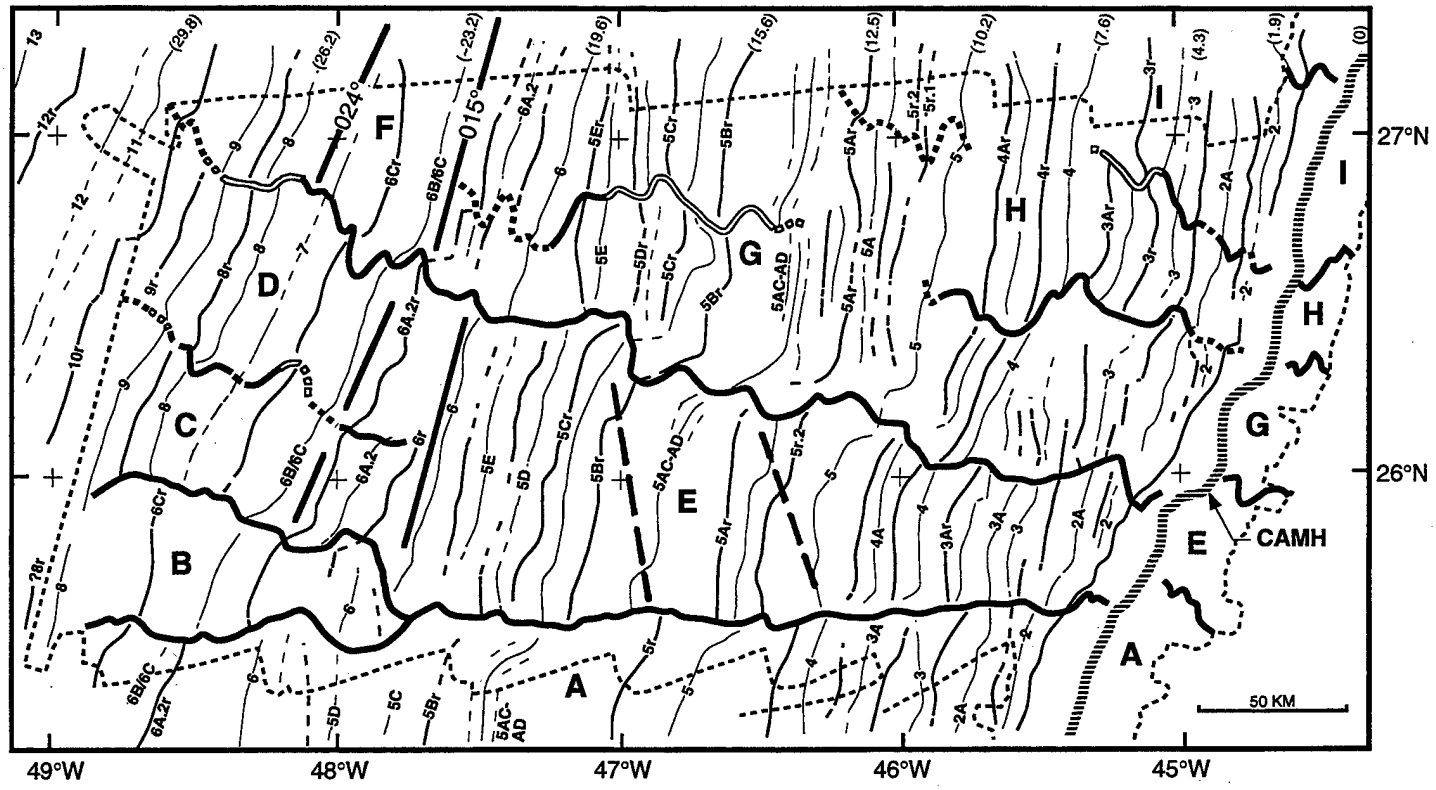

Figure 2

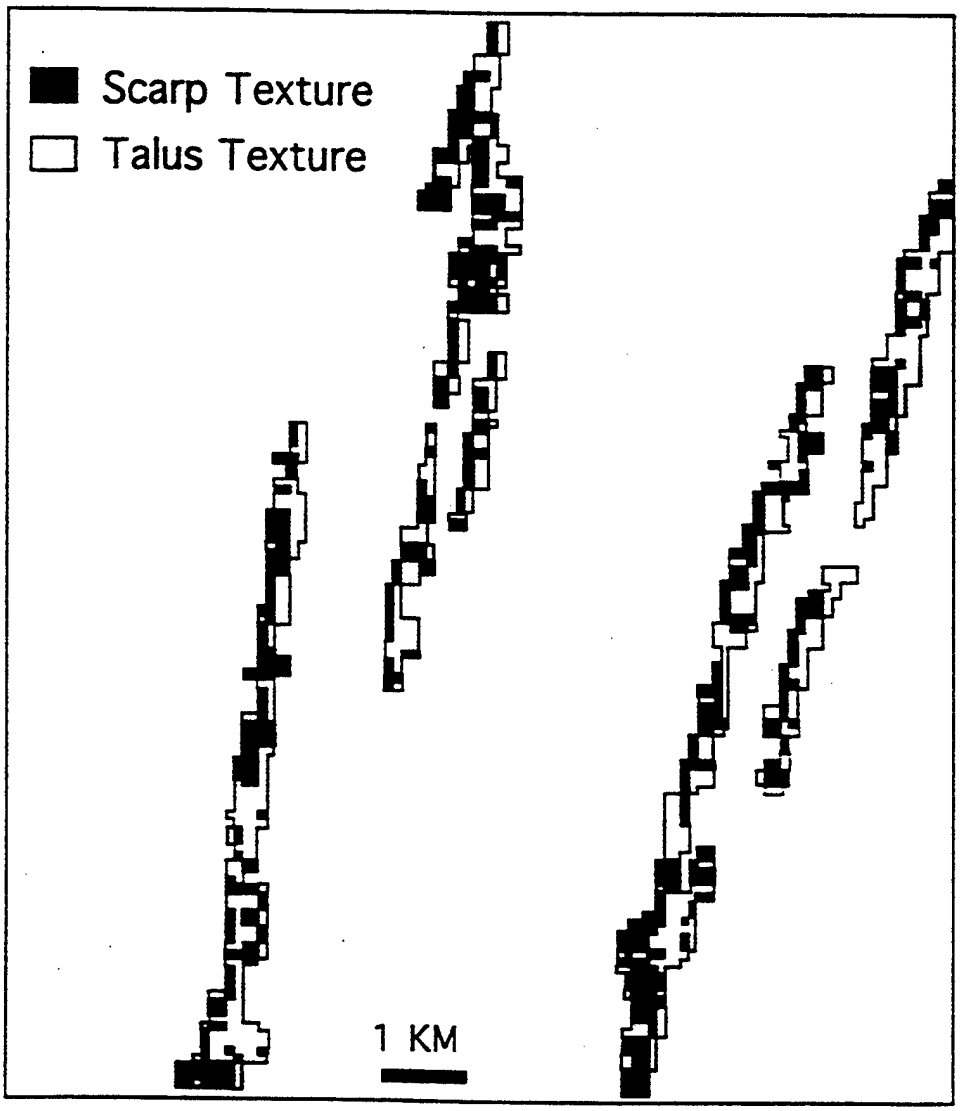

Pc = 0.74

Figure 3

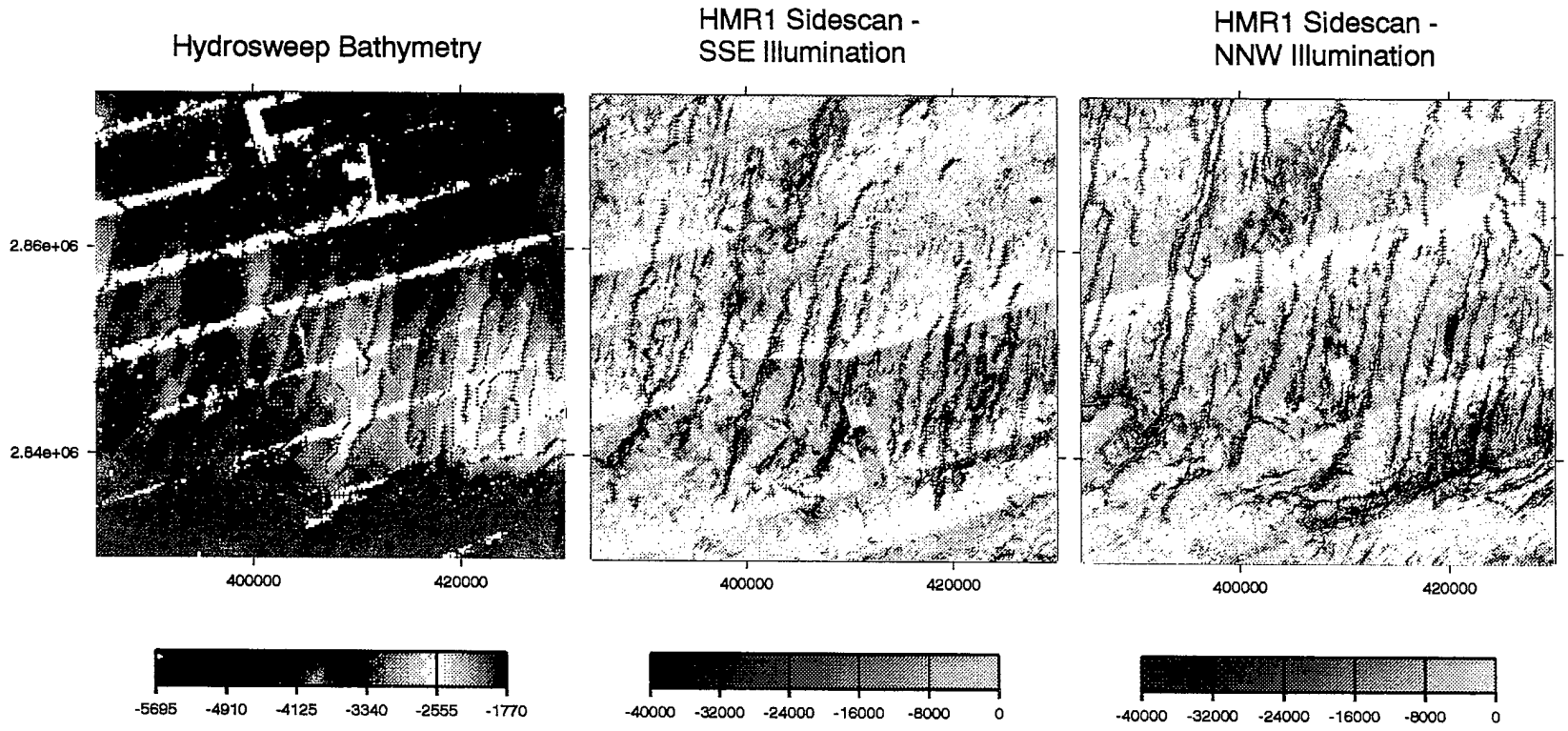
Hydrosweep Bathymetry
HMR1 Sidescan -
SSE Illumination
HMR1 Sidescan -
NNW Illumination
2.86e+06
2.84e+06
400000
420000
400000
420000
400000
420000
-5695
-4910
-4125
-3340
-2555
-1770
-40000
-32000
-24000
-16000
-8000
0
-40000
-32000
-24000
-16000
-8000
0

Figure 4

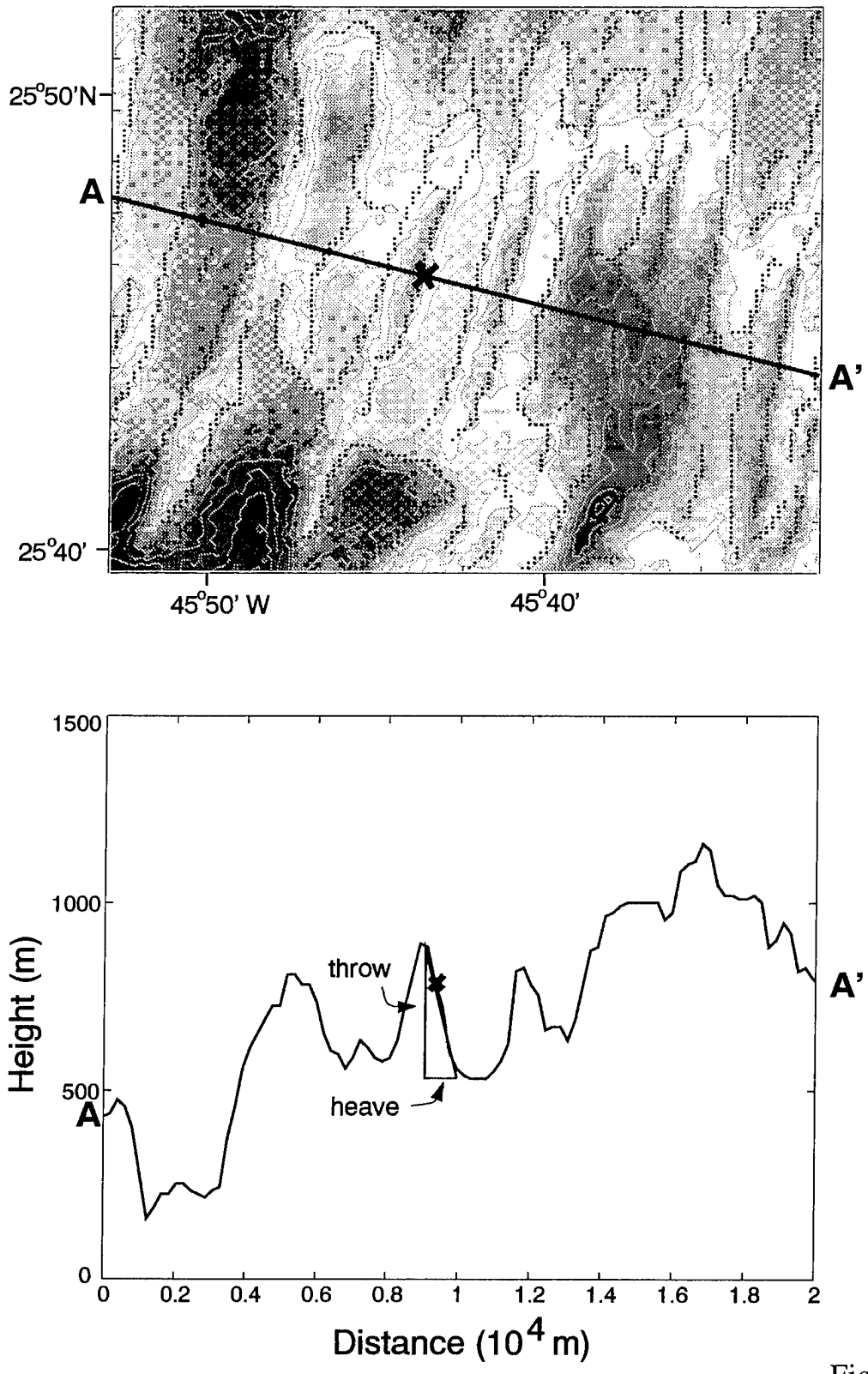
25°50'N
A
A'
25°40'
45°50' W
45°40'
1500
1000
500
0
Height (m)
throw
heave
A
A'
0
0.2
0.4
0.6
0.8
1
1.2
1.4
1.6
1.8
2
Distance (10^4 m)

Figure 5

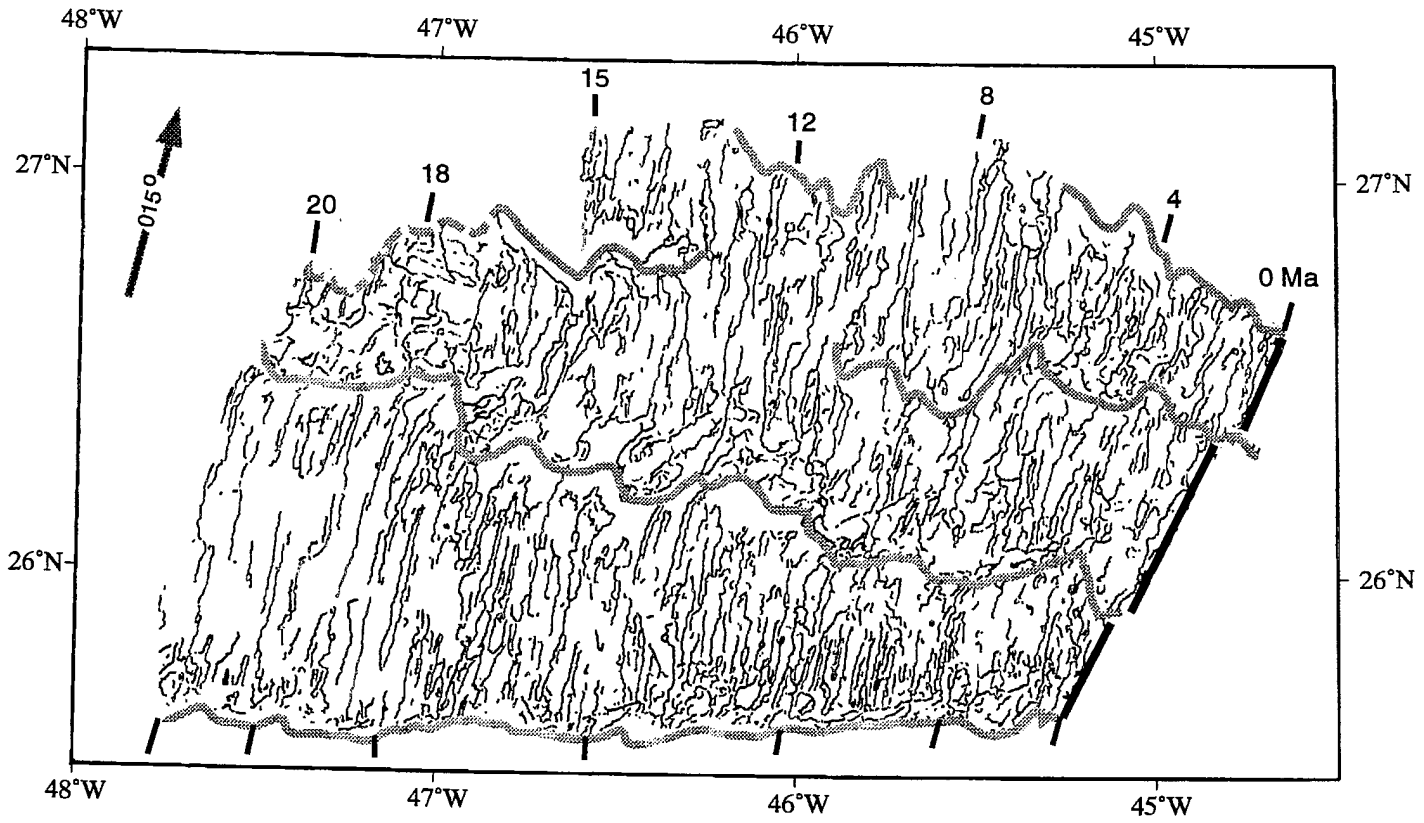

Figure 6

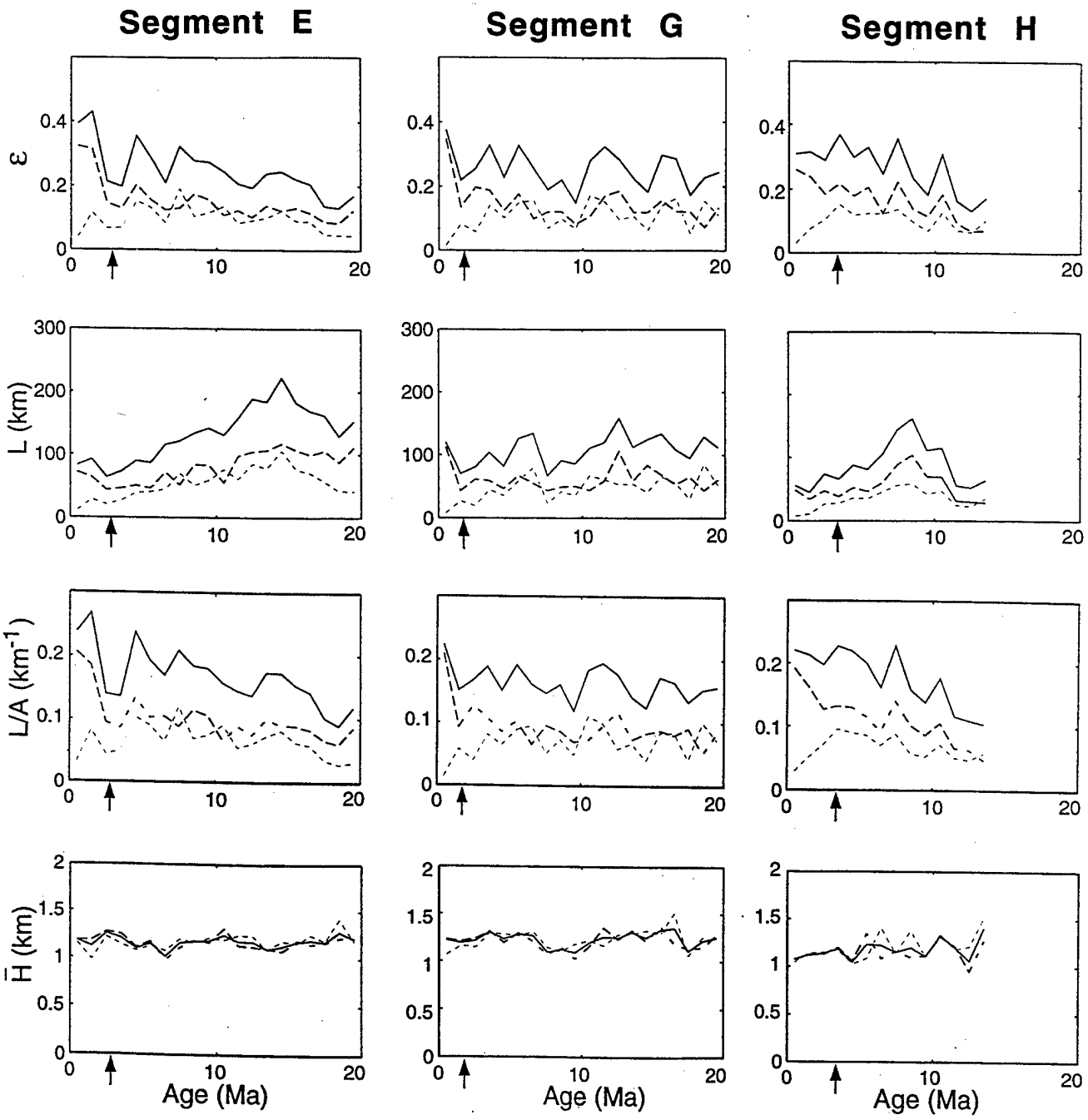
Segment E
Segment G
Segment H
ε
L (km)
L/A (km⁻¹)
H̄ (km)
Age (Ma)
Age (Ma)
Age (Ma)

Figure 7

RIFT-VALLEY WALL

Horizontal Views into Fault Faces

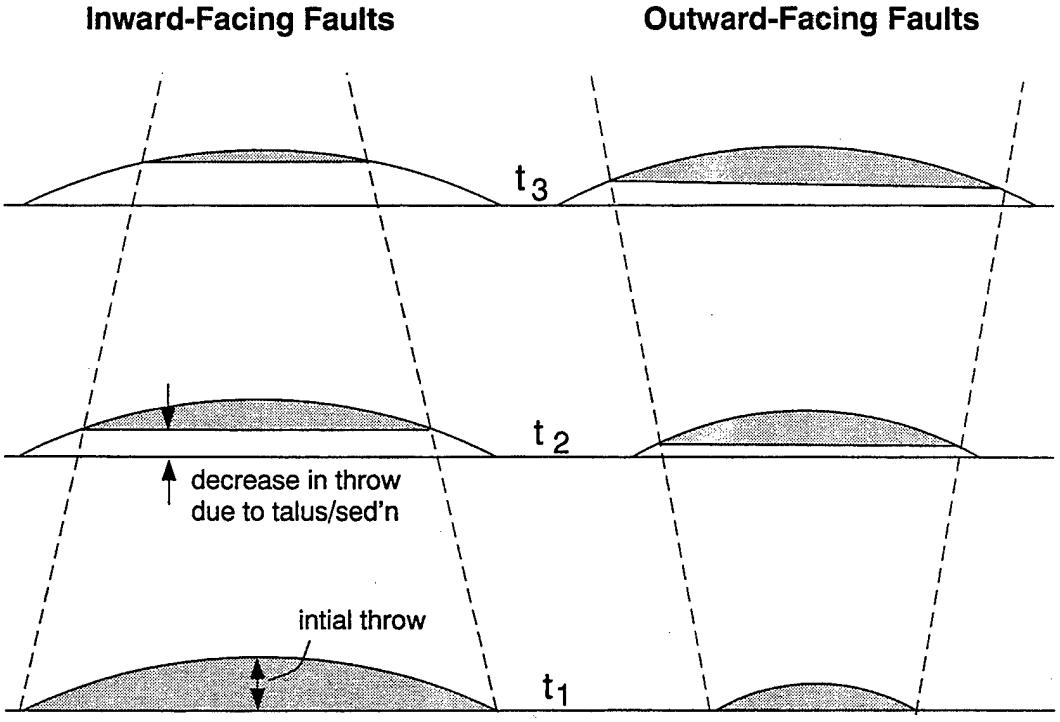

DISPLACEMENT CONSTANT
WITH TIME (INACTIVE FAULTS)

DISPLACEMENT INCREASES
WITH TIME (ACTIVE FAULTS)

Throw ↓ } change ~ proportionately { Throw ↓

Dip ↓ Dip ↓

H ~ constant H ~ constant

L and L/A ↓ L and L/A ↑

ε ↓ ε ↑

Figure 8

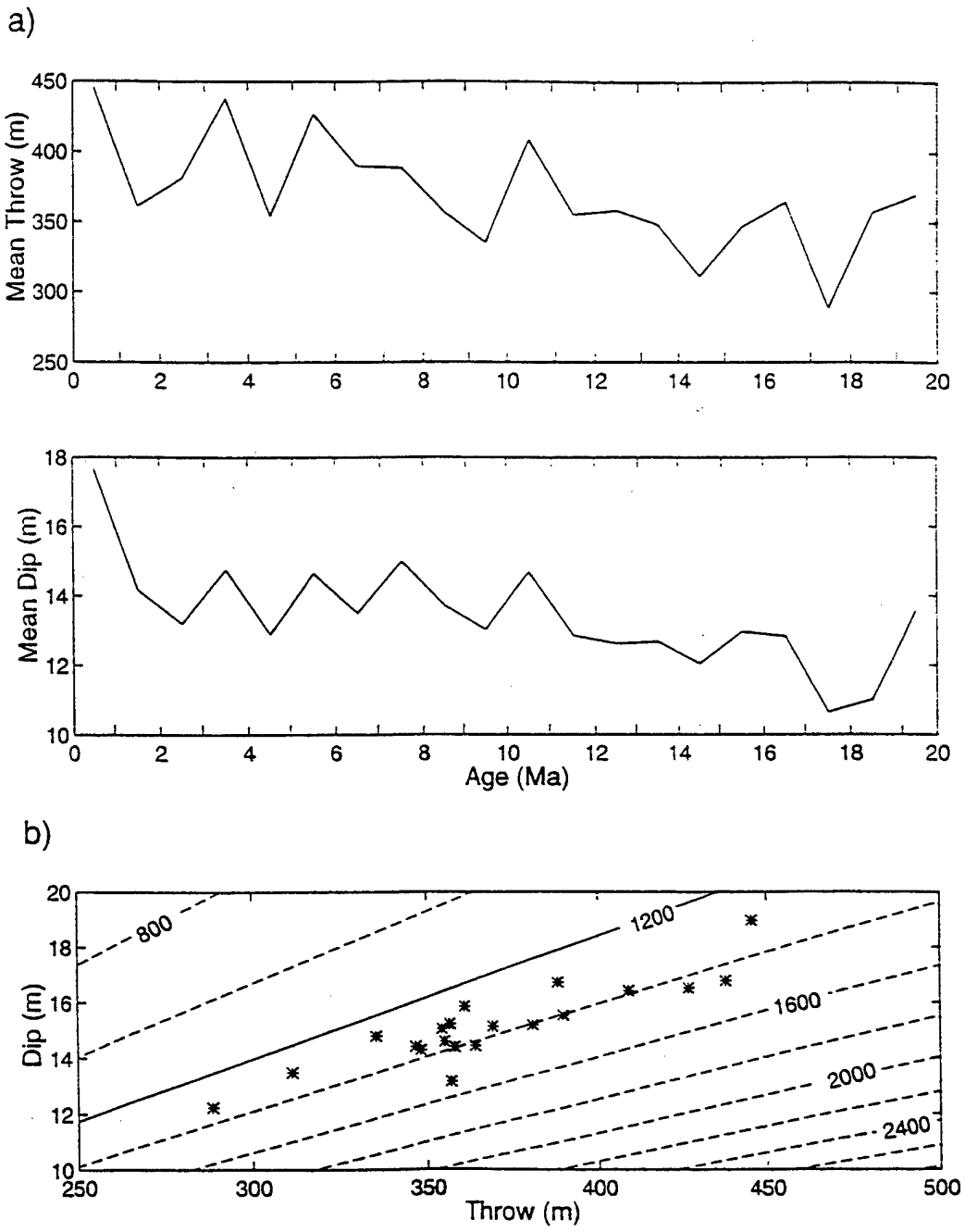
a)
Mean Throw (m)
450
400
350
300
250
0
2
4
6
8
10
12
14
16
18
20
Mean Dip (m)
18
16
14
12
10
Age (Ma)
b)
Dip (m)
20
18
16
14
12
10
800
1200
1600
2000
2400
250
300
350
400
450
500
Throw (m)

Figure 9

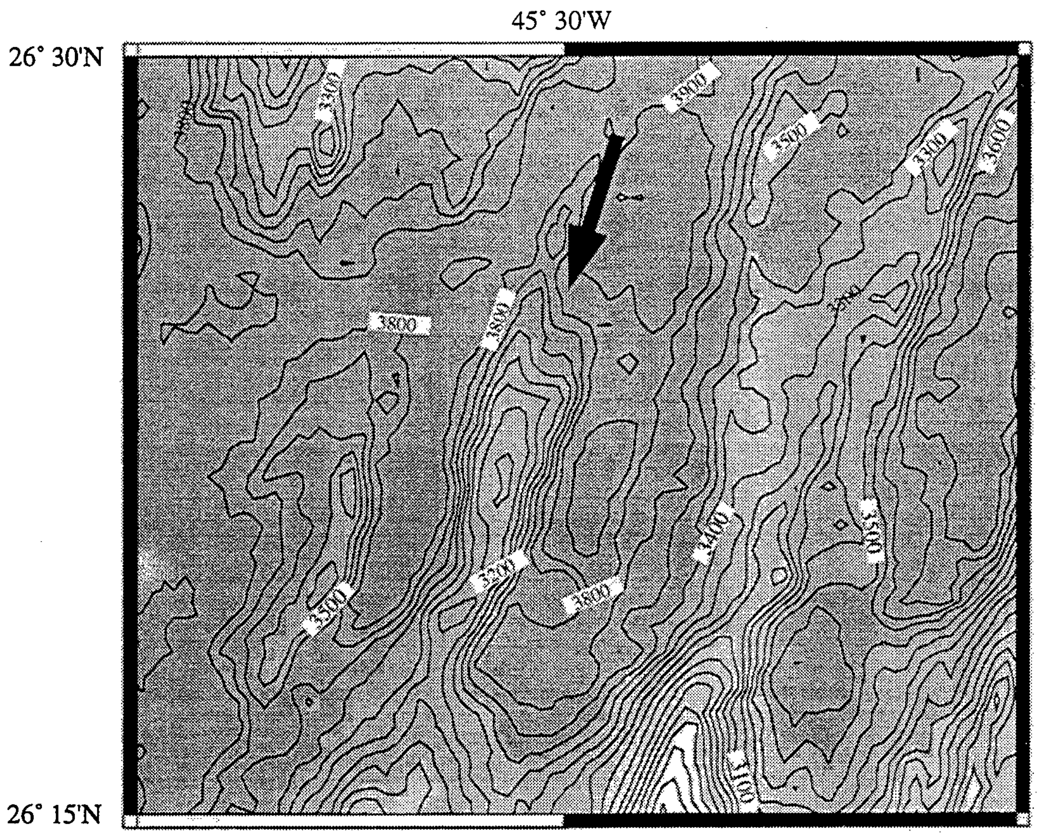
45° 30'W
26° 30'N
26° 15'N
3300
3900
3500
3300
3600
3800
3800
3200
3800
3400
3500
3500
3100

Figure 10

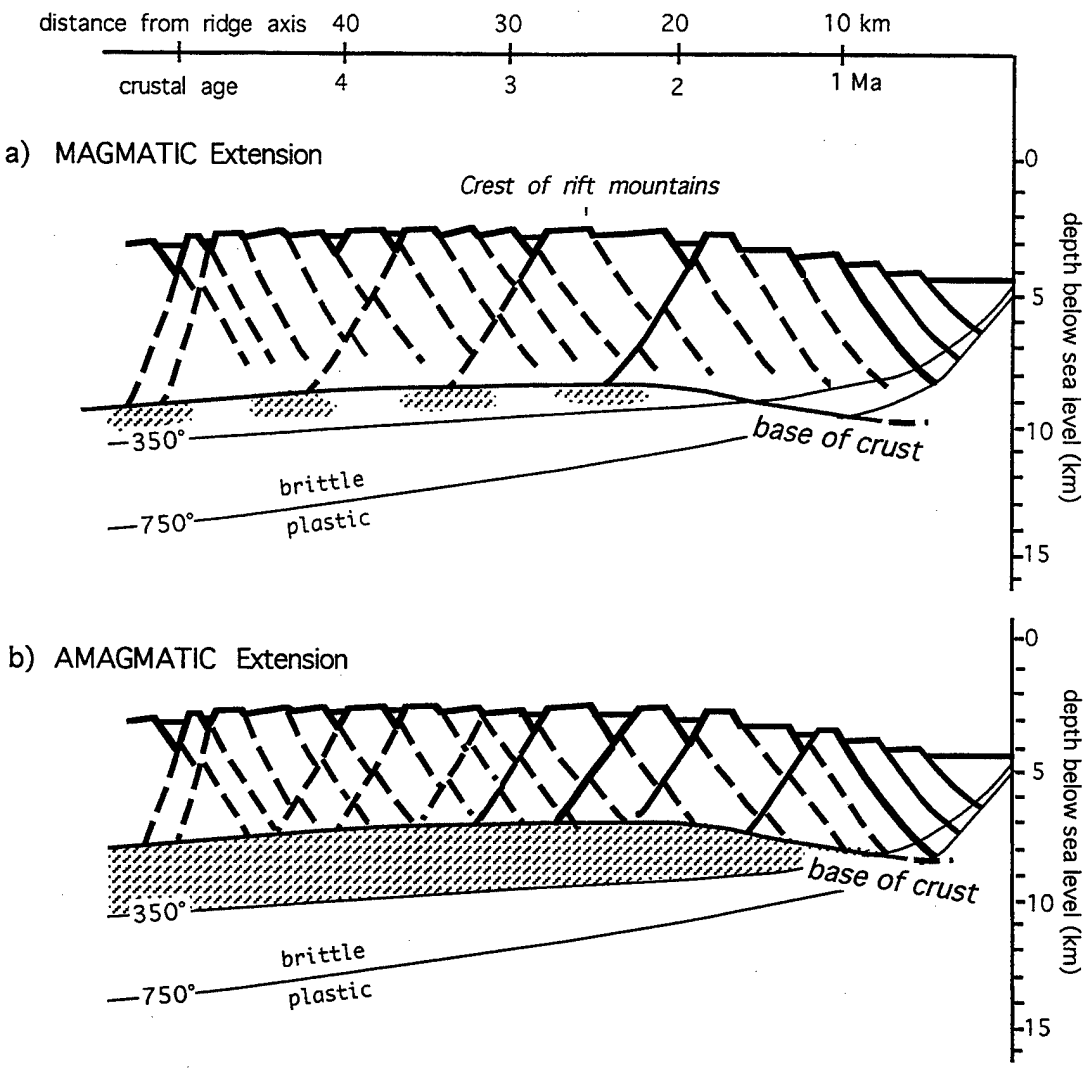
distance from ridge axis 40 30 20 10 km
crustal age 4 3 2 1 Ma
a) MAGMATIC Extension
Crest of rift mountains
0
5
10
15
depth below sea level (km)
350°
base of crust
brittle
plastic
750°
b) AMAGMATIC Extension
0
5
10
15
depth below sea level (km)
base of crust
350°
brittle
plastic
750°

Figure 11

MID-ATLANTIC RIDGE SEAMOUNTS, 26°N

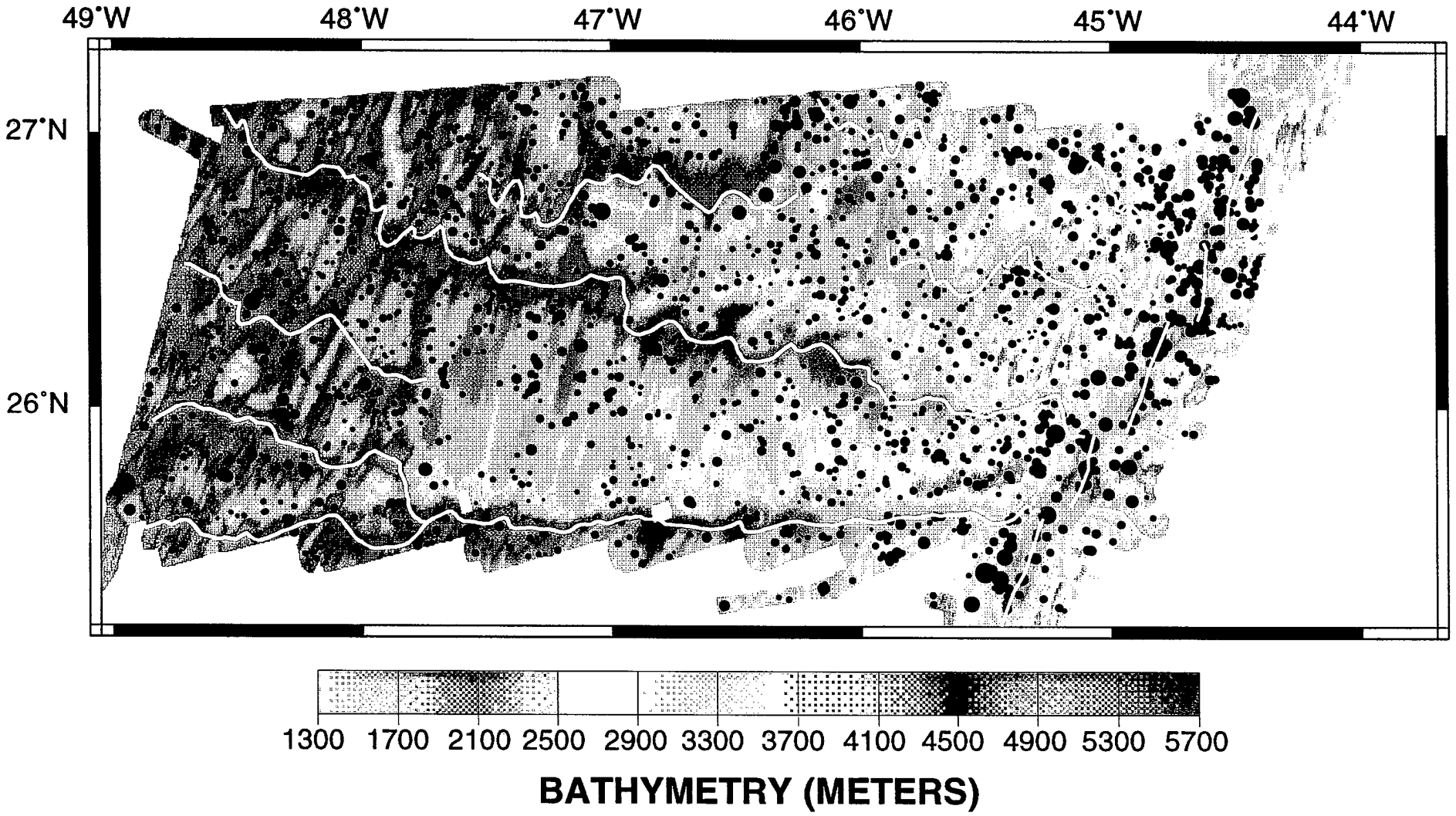

Figure 12

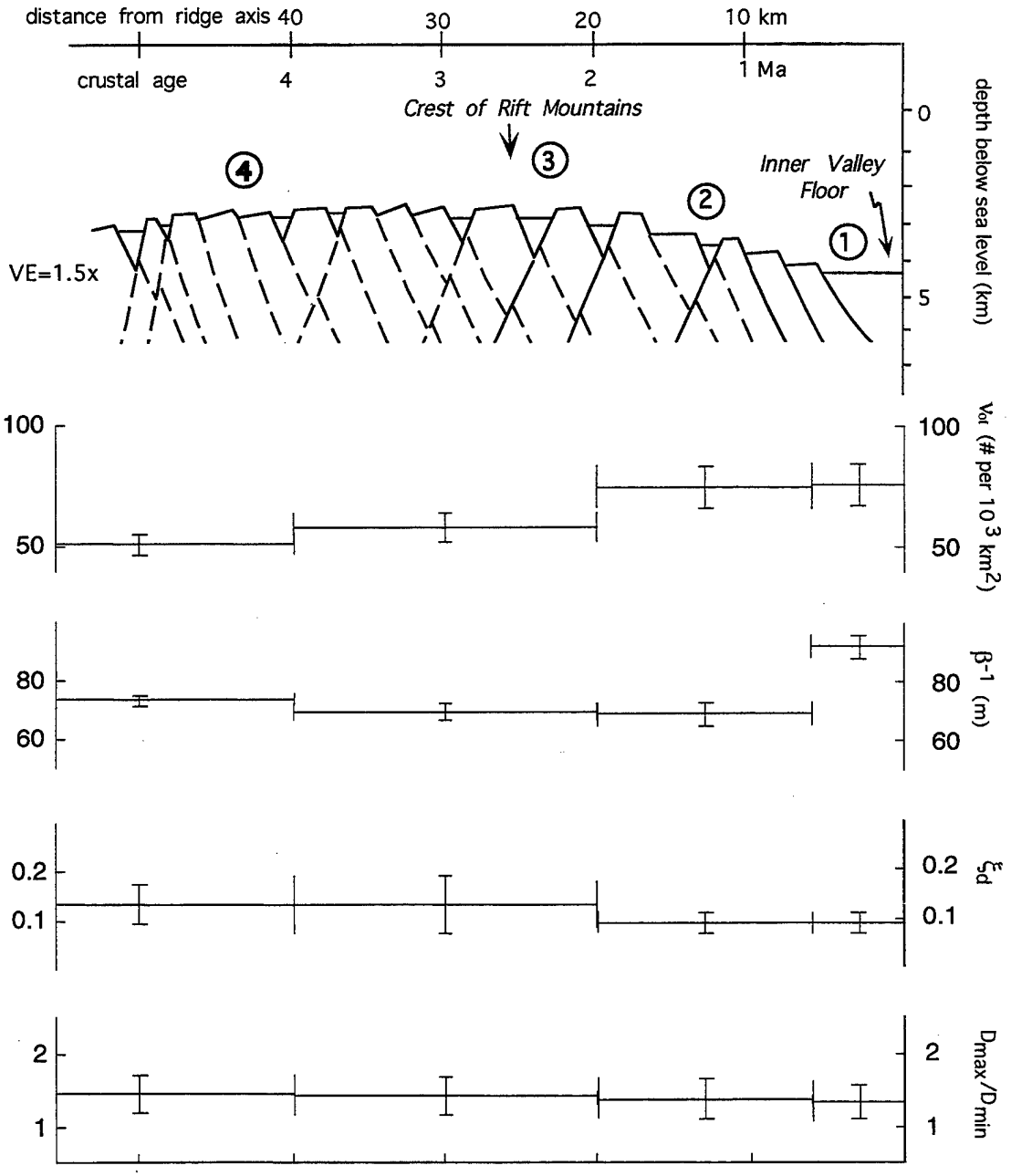
distance from ridge axis 40
30
20
10 km
crustal age
4
3
2
1 Ma
Crest of Rift Mountains
Inner Valley Floor
VE=1.5x
depth below sea level (km)
0
5
100
50
V_{ol} (# per 10^3 km^2)
80
60
β^{-1} (m)
0.2
0.1
ξ_d
2
1
D_{max}/D_{min}

Figure 13

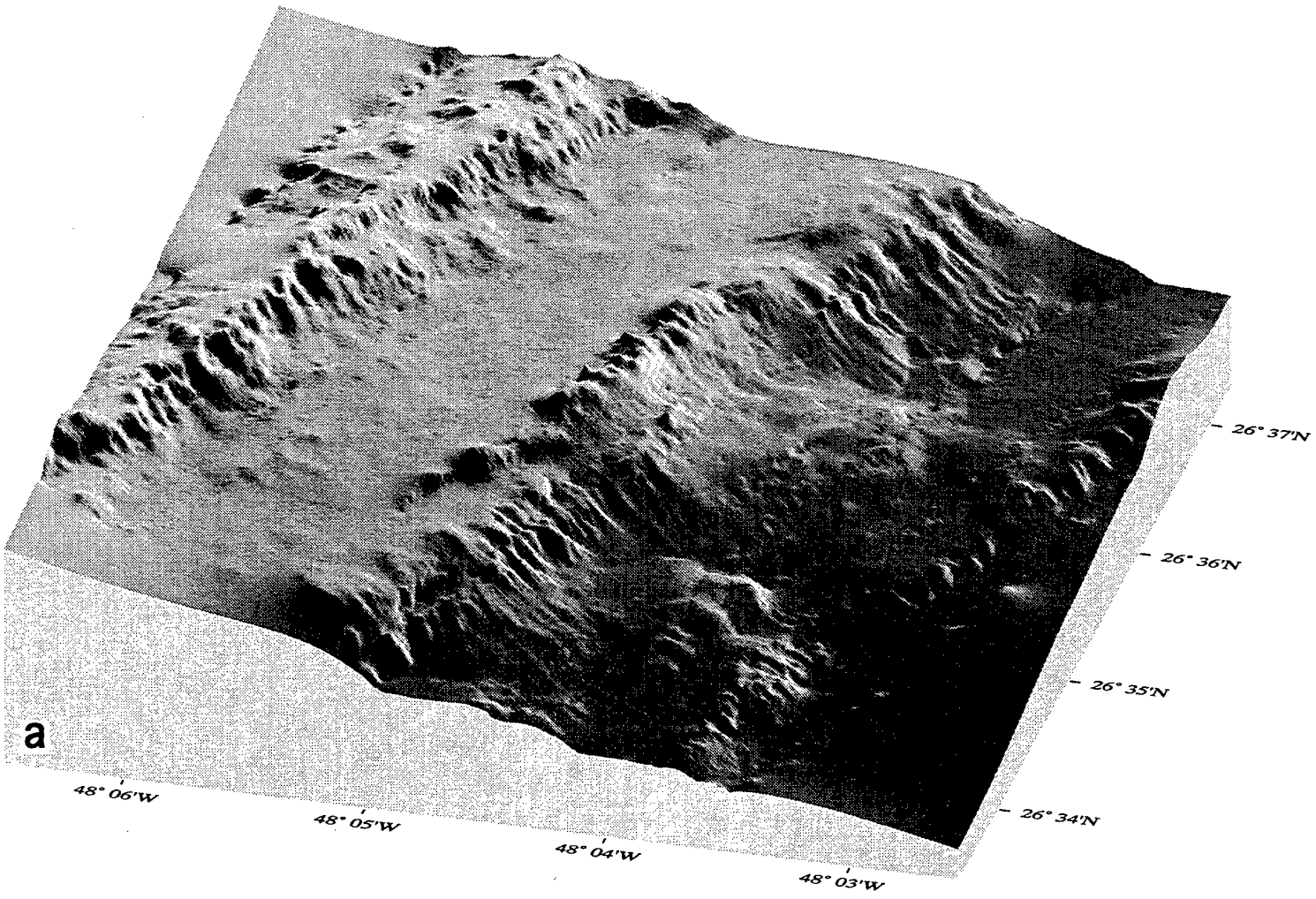
a
48° 06'W
48° 05'W
48° 04'W
48° 03'W
26° 37'N
26° 36'N
26° 35'N
26° 34'N

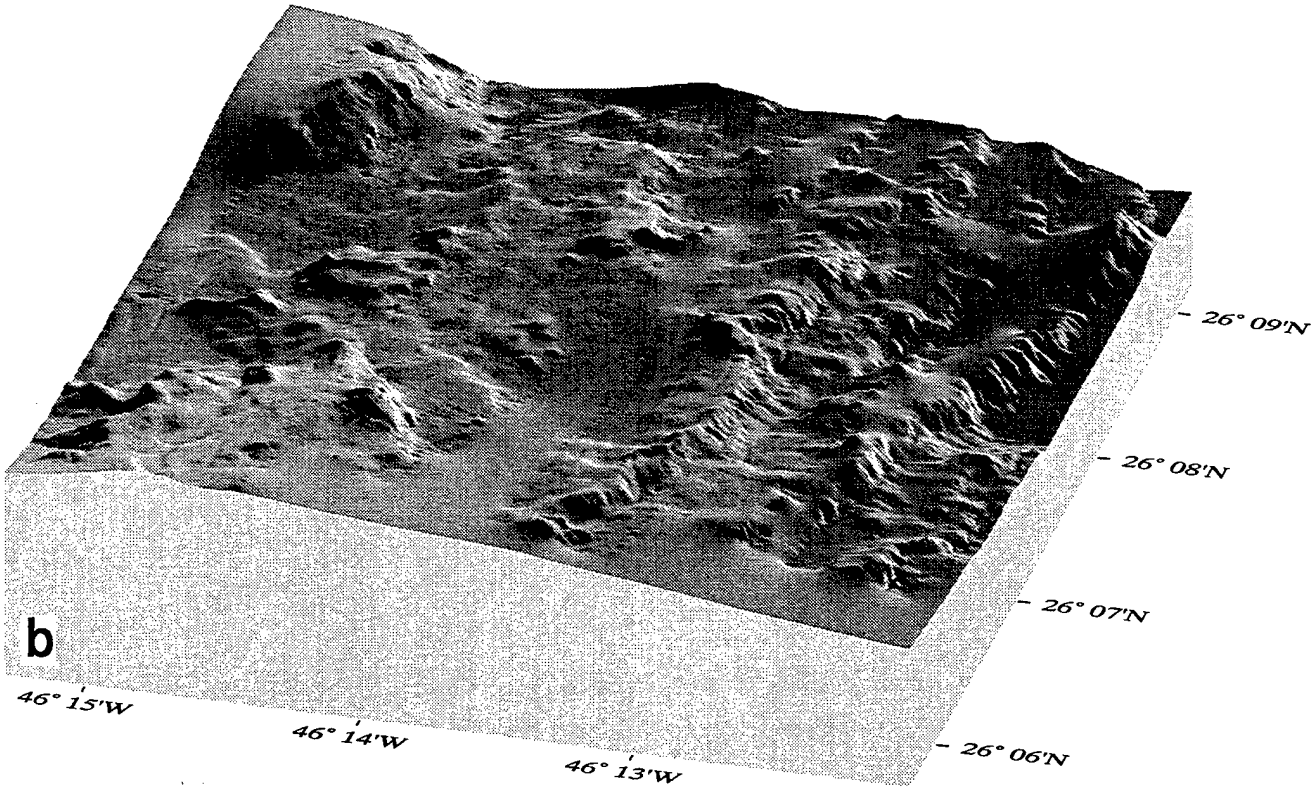
b
46° 15'W
46° 14'W
46° 13'W
26° 09'N
26° 08'N
26° 07'N
26° 06'N

Figure 14

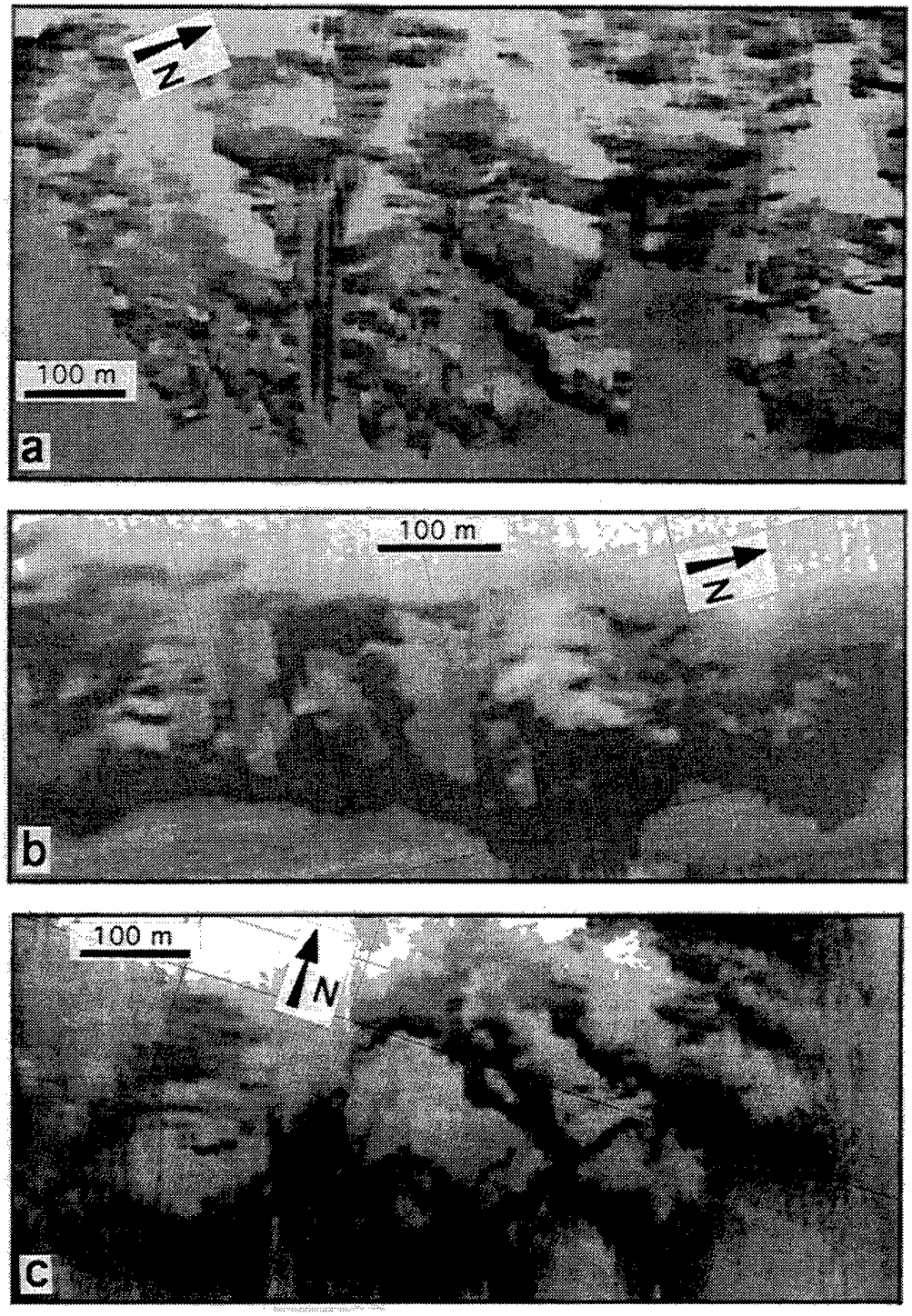

Figure 15